AN INVESTIGATION INTO THE DEFORMATION AND TEARING OF THIN CIRCULAR PLATES SUBJECTED TO IMPULSIVE LOADS

by

RG TEELING-SMITH

1989

Submitted to the University of Cape Town
in partial fulfilment of the requirements for
the degree of master of science

DECLARATION

I, GRAEME TEELING-SMITH, declare that this thesis is essentially my own work and has not been submitted in this or in a similar form for a degree at any other university.

ABSTRACT

This investigation, primarily experimental, examines the failure of circular plates subjected to impulsive velocities. The experiments are conducted on fully clamped circular steel plates subjected to a uniformly distributed impulse.

The strain-rate-sensitive mild steel plates fail with mode I (large ductile deformation), mode II (tensile-tearing and deformation) and mode III (transverse-shear) failure modes. The impulse is measured by means of a ballistic pendulum upon which the test plates are attached. During mode II and mode III failure the complete circumferential tearing of the test plate produces a circular disc. The velocity of this disc is recorded.

An energy analysis is performed on the test results and an energy balance equation is formulated.

$$E_{input} = E_{deformation} + E_{tearing} + E_{disc}$$

The input and disc energies are obtained from the experimental measurements and the deformation energy is predicted by using the final deformed height and a shape function together with a rigid-plastic energy analysis adopted by Duffey [1]. $E_{tearing}$ refers to the energy for tensile-tearing in mode II failure or the energy for transverse-shear in mode III failure. Good correlation is found and the experiments show good repeatability.

The threshold velocities for the onset of failure modes II and III are given.

ACKNOWLEDGEMENTS

The author wishes to thank the following:

Dr GN Nurick: for his valued advice and support as well as his many hours spent preparing and detonating the explosive charges.

Mr G Bertuzzi: for his assistance and help in the explosive testing room.

Mr J Mayer: for his ideas and assistance with the electronic equipment.

Messrs MAH Batho, A Warburton and H Tomlinson: for preparing the required test equipment and test specimens.

Professor LP Adams and Miss A Tregidga: for their assistance in measuring the deformed plates.

Mrs S Creed: for her work in the preparation of the final copy of this thesis.

AECI (Pty) Limited for providing the explosive material.

The Department of Mechanical Engineering and the Foundation for Research Development for their financial assistance.

TABLE OF CONTENTS **Page**

Declaration		i
Abstract		ii
Acknowledgements		iv
Table of Contents		v
List of Figures		viii
List of Tables		xi
Nomenclature		xii
Chapter 1	**INTRODUCTION**	1
Chapter 2	**EXPERIMENTAL DETAILS**	4
2.1	INTRODUCTION	4
2.2	EXPERIMENTAL MEASUREMENTS	10
2.3	EXPERIMENTAL PROCEDURE	13
2.3.1	Plates and Clamping Fixture	13
2.3.2	Material Properties	13
2.3.3	Ballistic Pendulum	18
2.3.4	Explosive Material, Mass and Geometry	26
2.3.5	Determination of Plate Velocity After Tearing	31
2.4	CIRCULAR DISC ENTRAPMENT	33
2.5	TEST RESULTS	34
2.5.1	Experimental Reliability	34
2.5.2	Test Readings	36
2.5.2.1	Impulse	36
2.5.2.2	Velocity of circular disc	36
2.5.2.3	Measured deflection	37

2.5.2.4	Test results of uniaxial yield tests	37
2.5.2.5	Table of test data	38
2.6	EXPERIMENTAL OBSERVATIONS	53
Chapter 3	**THEORETICAL INVESTIGATION**	58
3.1	INTRODUCTION	58
3.2	ENERGY ANALYSIS	63
3.2.1	Introduction	63
3.2.2	Rigid Plastic Analysis	64
3.3	INFLUENCE OF MATERIAL STRAIN-RATE SENSITIVITY AND STRAIN HARDENING	66
3.4	SHAPE APPROXIMATION FUNCTIONS	69
Chapter 4	**RESULTS**	72
Chapter 5	**DISCUSSION AND CONCLUSIONS**	87
Chapter 6	**RECOMMENDATIONS**	90
REFERENCES		91

APPENDICES

A - Tensile Tests

B - Rigid Plastic Analysis

C - Dynamic Yield Stress Values

D - Prediction of a Polynomial using Stirling's Formula

E - Confidence Limits of Slope and Least Squares Line

F - Calculation of maximum strain rate

G - Courses completed for partial fulfilment of the requirements for the degree of Master of Science

LIST OF FIGURES **Page**

Figure 2.1	Permanent profiles of impulsively loaded plates showing the three failure modes	7
Figure 2.2	Photograph of test plates illustrating the transition between the 3 modes	8
Figure 2.3	Test plate and clamping device	14
Figure 2.4a	Uniaxial stress strain tensile test for Sheet I	15
Figure 2.4b	Uniaxial stress strain tensile test for Sheet II	16
Figure 2.5	Experimental arrangement	20
Figure 2.6	Ballistic pendulum geometry	22
Figure 2.7	Explosive configuration	28
Figure 2.8	Graph of mass of explosive versus impulse	30
Figure 2.9	Electrical circuit for velocity measurement	32
Figure 2.10a	Typical oscilloscope time measurement 250901	39
Figure 2.10b	Typical oscilloscope time measurement 250903	40
Figure 2.10c	Typical oscilloscope time measurement 250906	41
Figure 2.10d	Typical oscilloscope time measurement 270903	42

Figure 2.11a	Typical contour plot and deformed profiles Test No 0410006 (deformation only)	43
Figure 2.11b	Typical contour plot and deformed profiles Test No 051005 (iniation of tearing)	44
Figure 2.11c	Typical contour plot and deformed profiles Test No 051001 (complete tearing)	45
Figure 2.11d	Typical contour plot and deformed profiles Test No 250902 (complete tearing)	46
Figure 2.11e	Typical contour plot and deformed profiles Test No 061001 (complete tearing)	47
Figure 2.11f	Typical contour plot and deformed profiles Test No 061004 (complete tearing)	48
Figure 2.12a	Typical three dimensional plots of deformed plates (deformation only)	49
Figure 2.12b	Typical three dimensional plots of deformed plates (partial and complete tearing)	50
Figure 2.12c	Typical three dimensional plots of deformed plates (complete tearing)	51
Figure 2.13a	Photograph showing the wrinkling of the metal disc	54
Figure 2.13b	Illustration of the symmetrical nature of the ears associated with wrinkling of the metal disc	55
Figure 2.14	Photograph showing the deformation of the clamping holes	57
Figure 4.1	Graph of deflection-thickness ratio vs dimensionless No ϕ with a least squares	74

	correlation	
Figure 4.2a	Comparison between experimental and predicted shape functions - test no 041006 (I = 13,28 N.s)	76
Figure 4.2b	Comparison between experimental and predicted shape functions - test no 041007 (I = 24,56 N.s)	77
Figure 4.3	Graph of energy versus dimensionless no ϕ	82
Figure 4.4	Graph of energy vs dimensionless no ϕ showing the 3 modes of failure	83
Figure 4.5	Graph of energy vs dimensionless no ϕ showing a 90% confidence range of correlation	85
Figure B.1	Clamped circular plate after deformation	97

LIST OF TABLES **Page**

Table 2.1	Test plate dimensions and material properties	18
Table 2.2	Ballistic pendulum details	25
Table 2.3	Test data	52
Table 3.1	Predicted shape functions	71
Table 4.1	Comparison between deformation energy and input energy for mode 1 type failure	79

NOMENCLATURE

A	Area of plate
E	Energy
E_ρ	Total plastic strain energy
I	Total impulse
R	Radius of plate
R_o	Radius of plate over which impulse is imparted
V	Volume of plate
V_o	Initial velocity
V_{disc}	Velocity of circular disc
X	Bending strain in plate per unit length
Z	Distance from plate middle surface
n	Material constant
m	Mass of circular disc
r	Distance in radial direction
t	Plate thickness
t_f	Final response time
u	Displacement in radial direction
$\phi(r)$	Mode shape function
$\dot{\varepsilon}$	Strain rate
$\dot{\varepsilon}_o$	Strain rate material constant
$\dot{\varepsilon}_r$	Radial strain rate
ω	Vertical displacement of the plate
ω_o	Maximum displacement of the centre of the plate
ν	Poisson's ratio

ρ	Density of plate
σ_y	Yield stress of plate
σ_o	Static yield stress
σ_o^1	Dynamic yield stress
$\sigma_{\theta\theta}$, $\varepsilon_{\theta\theta}$	Stress and strain in circumferential direction
σ_{rr}, ε_{rr}	Stress and strain in meridional direction

CHAPTER 1 - INTRODUCTION

A primarily experimental investigation on the deformation and failure of clamped circular plates subjected to impulsive loading is presented in this study. The first found mention of different failure modes was by Menkes and Opat [2] on fully clamped beams loaded impulsively. The three damage modes are major inelastic deformation, tearing at the extreme fibre, and transverse shear at the support. These failure modes are identified in the experimental work performed in this thesis and an energy analysis is performed in order to determine the critical impulsive loads for the onset of these different failure modes.

Chapter 2 gives an explanation of the experimental details, with the first section giving a summary of the previous experimental work. Three types of impulsive loading are mentioned, namely when the structure is subjected to air pressure waves created by an air-blast, underwater explosive forming and direct impulsive loading using plastic sheet explosives. These investigations were concerned with the deformation of the structure and looked at the final deformed shape and the deflection-time history. The experiments are described in detail and measurements are taken to determine the applied impulse, the deformed shape of the plate, the final mid-point deflection, and the velocity of the metal disc where necessary. The metal disc being defined as that portion of the test plate which leaves the clamping rig after complete tearing (mode II

and III failure) has taken place along the entire circumference of the clamped boundary. Deflections of up to 30mm ($\frac{\delta}{t}$ = 18.75) are observed and where appropriate disc velocities of between 100 and 425ms^{-1} are measured.

The tests are carried out on mild steel plates which are assumed to be rigid-viscoplastic. The Cowper-Symonds relation is used for the computation of the dynamic and static yield stresses where required.

Chapter 2 concludes by commenting on certain experimental observations. These include the nature of the deformation of the clamping holes during mode I and mode II failures and the presence of symmetrical wrinkling of the metal disc when the impulse is between the critical values associated with mode II and mode III failures.

A theoretical investigation is presented in Chapter 3 with the study of the energy solution adopted by Duffey [1] using as his basis a rigid-plastic analysis procedure. The aim being to determine a way of estimating the energy required for the deformation of the circular plate. The final solution involved the use of an appropriate shape function, a number of which are given at the end of the chapter. A method for determining the dynamic yield stress required for the energy calculations is also presented.

The experimental and theoretical results are presented in Chapter 4. The energy results are compared with previous work on the deformation of plates and the different shape functions are compared with experimentally measured shapes. From the analysis of the experimental results a relationship is developed between the deflection-thickness ratio and ϕ. An empirical relationship is also developed between energy and ϕ. ϕ is a function of impulse, plate geometry and dimensions and material properties. The threshold values for the onset of mode II and mode III failures are determined from observation of the experimental results.

A discussion of the results is presented in Chapter 5. Good correlation is found between the experimental results with a reliable means of determining the energies of deformation and tearing.

Chapter 6 concludes this thesis with recommendations for future work.

Pressure waves created by an air-blast is the second type that has been reported and Noble et al [4] in 1964 used it in the determination of the efficiency of energy transfer in the explosive forming of sheet metal components.

Nurick [3] reported that the third type of impulsive loading involving the detonation of sheet explosives and a ballistic pendulum was first investigated by Humphreys in 1965. Humphreys found that the burn rate of the explosive was $6700 m.s^{-1}$ which is greater than the speed of sound in carbon steel of $5150 m.s^{-1}$ (Johnson [5]) and it was therefore felt that the loading could be approximated to that of an instantaneous impulsive load. Nurick [3] found that the response time for the deformation of the mild steel plates was 140-190μs and the natural period of the ballistic pendulum was 3,21 seconds. Thus all plastic deformation takes place before the pendulum has moved. Therefore the recorded deflection of the pendulum gives a direct indication of the maximum potential energy in plastic work. The deflection is used to calculate the velocity of the ballistic pendulum and thereby giving an accurate indication of the applied impulsive load.

The only found mention of a certain degree of tearing in a small portion (approximately one-tenth) of the

boundary perimeter has been by Nurick and Martin [6] who observed that this partial tearing along the clamped boundary occurred at an impulse of 15,6 Ns. Wierzbicki et al [7], Duffey [1], and Bodner et al [8] have all carried out successful work on the deformation of circular plates with a sheet explosive blast providing the impulsive load, but have only dealt with deflection-thickness ratio's which are less than the maximum of 12 observed by Nurick [3].

Work has also been done on explosively loaded clamped beams and in 1973 Menkes et al [2] found that as the impulse increased, three distinctly different damage modes were noted:

Mode I	Large inelastic deformation
Mode II	Tearing (tensile failure) in outer fibres, at or over the support
Mode III	Transverse shear failure at the support.

These three failure modes are shown schematically in Figure 2.1 and a photograph of several tests plates showing the transition between the failure modes is shown in Figure 2.2.

In mode I failure the extent of the damage is described by the amount of residual central deflection, for mode II failure the threshold is taken as that

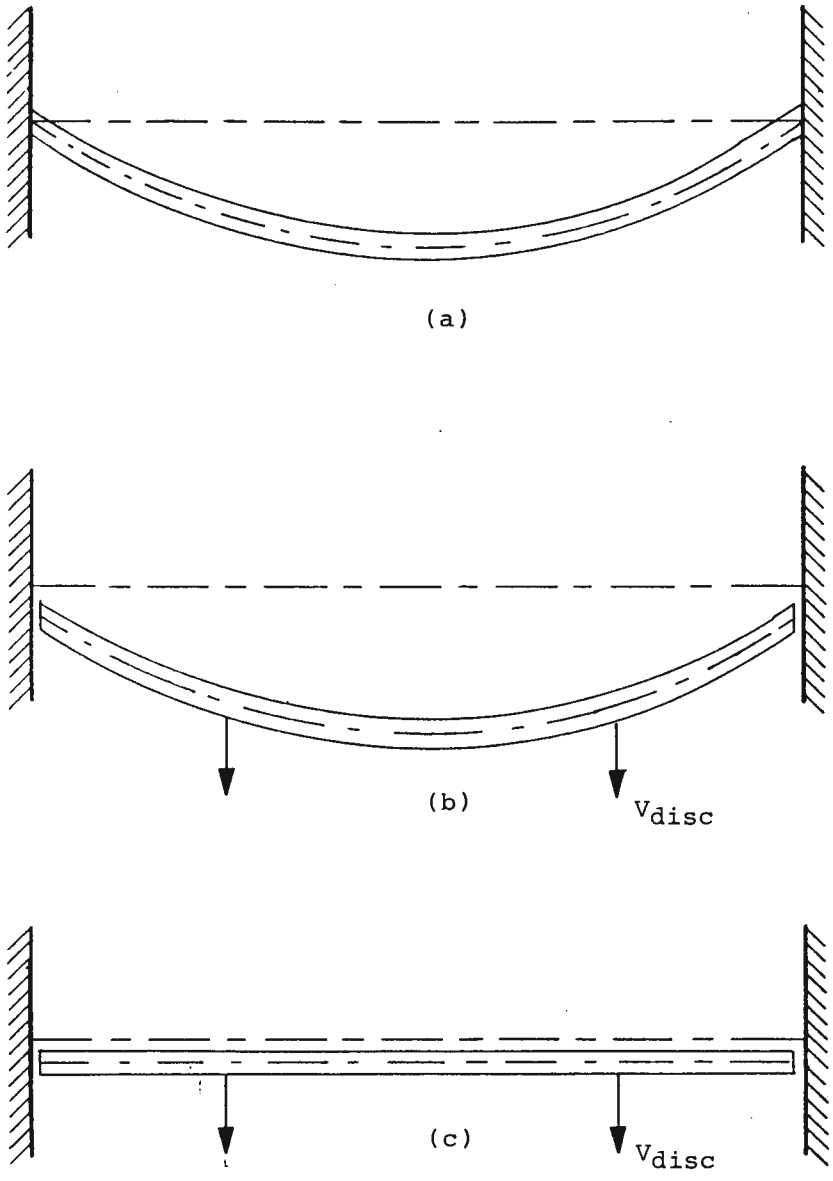

FIGURE 2.1 PERMANENT PROFILES OF IMPULSIVELY LOADED PLATES SHOWING THE 3 FAILURE MODES:
(a) MODE I, LARGE DEFORMATIONS
(b) MODE 2, TENSILE TEARING AT SUPPORTS
(c) MODE 3, TRANSVERSE SHEAR FAILURE AT SUPPORTS (Ref (17))

041006
I = 13,28 N.s

041007
I = 24,56 N.s

041008
I = 29,24 N.s

220901
I = 32,66 N.s

250904
I = 39,38 N.s

061001
I = 39,56 N.s

061004
I = 49,64 N.s

FIGURE 2.2 PHOTOGRAPH OF TEST PLATES ILLUSTRATING THE TRANSITION BETWEEN THE FAILURE MODES

impulse intensity which first causes tearing and mode III is characterised by a well defined shear failure with no significant deformation in the severed central section.

Jones [9] also mentions these failure modes and attempts to estimate the threshold velocities at which failure due to either tensile tearing or shearing occurs at the supports of the beams. It should be noted that some of the beams in the experimental work by Menkes et al [2] exhibited failures which involved both the tearing and shearing modes when subjected to the impulsive velocities lying between the smallest velocities required for the onset of modes II and III failures. The simple rigid-plastic methods used by Jones [9] simply define the lowest or threshold impulsive velocities which are necessary to cause tensile tearing and pure shear failures at the supports respectively. The threshold velocity found by Jones [9] to be necessary for the onset of a mode III response in beams with rectangular cross sections was found to be constant for a given material and therefore independent of its dimensions. The only two variables affecting this threshold velocity were the uniaxial yield stress and the density of the material. The approximate theoretical methods used by Jones [9] were found to give reasonable agreement with the experimental tests of Menkes [2] on aluminium beams.

In 1988 Duffey [10] during investigations of the dynamic rupture of shells found that particularly for thin shells, considerable plasticity may occur before failure by material separation, so that the concepts of classical brittle fracture mechanics are not applicable for failure prediction. Also the fact that the deformations were found to be so localised at the supports suggest that these mode III beam results may apply (approximately) to shear failure in other structures.

2.2 EXPERIMENTAL MEASUREMENTS

For each experiment three measurements are needed. Firstly the measurement of the impulse is required as from this the initial velocity of the plate as well as the total energy input is determined. For the tests where complete tearing occurs the velocity of the circular disc is required thus enabling the excess kinetic energy to be calculated. The third measurement to be made after deformation and tearing have taken place is the final mid-point deflection of the plate and the shape of the deformation.

There are different ways of determining the impulse measurements. One way used by Duffey [1] and Florence [11] is to determine the impulse delivered in separate calibration tests by using coupons the same diameter, thickness and material as the plate, and loaded with identical explosive and attenuator systems. Duffey [1] measures the coupon velocity by means of an array of contact pins. Duffey [1] found that this method was reported by RD Krieg in 1967. Since the mass of the coupon is known, and the explosive is weighed in each case, determination of the velocity of the coupon allows the impulse per unit mass of the explosive to be calculated. The explosive is then carefully weighed in each test and the impulse delivered found by multiplying the appropriate specific impulse by the explosive mass. Bodner et al [12] took direct impulse measurements for each test. Nurick [13] found this second option to be the most desirable and reported that during his experimental testing he observed that the impulse per unit mass of charge depends not only on the charge mass but also on the geometry of the charge and the configuration adjacent to the specimen.

In determining the velocity of the circular disc after complete tearing has taken place it is important to adopt a simple but accurate device. The first method considered, is a light interference method in which

two beams of light are placed at a known distance from each other and the test plate, as the disc passes through, the beams are broken and measurements taken. The second method deliberated is to use high speed photography and by determining the distance moved by the disc between successive frames the velocity can be determined. These two options although in theory appear to be highly desirable, are ruled out as in both cases the flash caused by the explosion would interfere with the light beams and also with the photographic equipment. The equipment would also have to be connected to the pendulum to obtain velocities relative to the motion of the pendulum and because of the extreme forces caused by the explosions, damage could possibly be caused to the expensive equipment.

The method adopted in this experimentation is simple yet effective. The process involves the breaking of two fuse wires with a small voltage applied across each one. As each wire is broken a signal is sent to a digital memoryscope where the time take for the disc to travel a certain distance is measured.

Uniaxial yield properties of the plate material are measured by performing a number of tensile tests and obtaining stress-strain curves for different strain rates.

2.3 EXPERIMENTAL PROCEDURE

2.3.1 Plates and Clamping Fixture

All the test plates are 200mm square and are clamped between two 20mm thick heavy steel plates by means of eight M12 bolts. Both the heavy clamping plates have a 100mm diameter circular hole in the centre through which the thin test plates can deform when loaded impulsively. Figure 2.3 shows the plate and the clamping device with the position of the clamping bolts.

The 1,6mm thick test plates are cut from two sheets of cold rolled mild steel and ten tensile specimens are cut from each sheet.

2.3.2 Material Properties

The tensile tests are performed on the two sets of mild steel specimens at strain rates between $3{,}33 \times 10^{-4}$ sec^{-1} and $1{,}33 \times 10^{-1}$ sec^{-1}. Typical stress-strain curves for the two materials are given in Figures 2.4(a) and 2.4(b). In both cases a distinct yield stress can be identified and values of the dynamic yield stress and the ultimate tensile stress can be measured. The static yield stress is computed using the results of the tests and substituting into

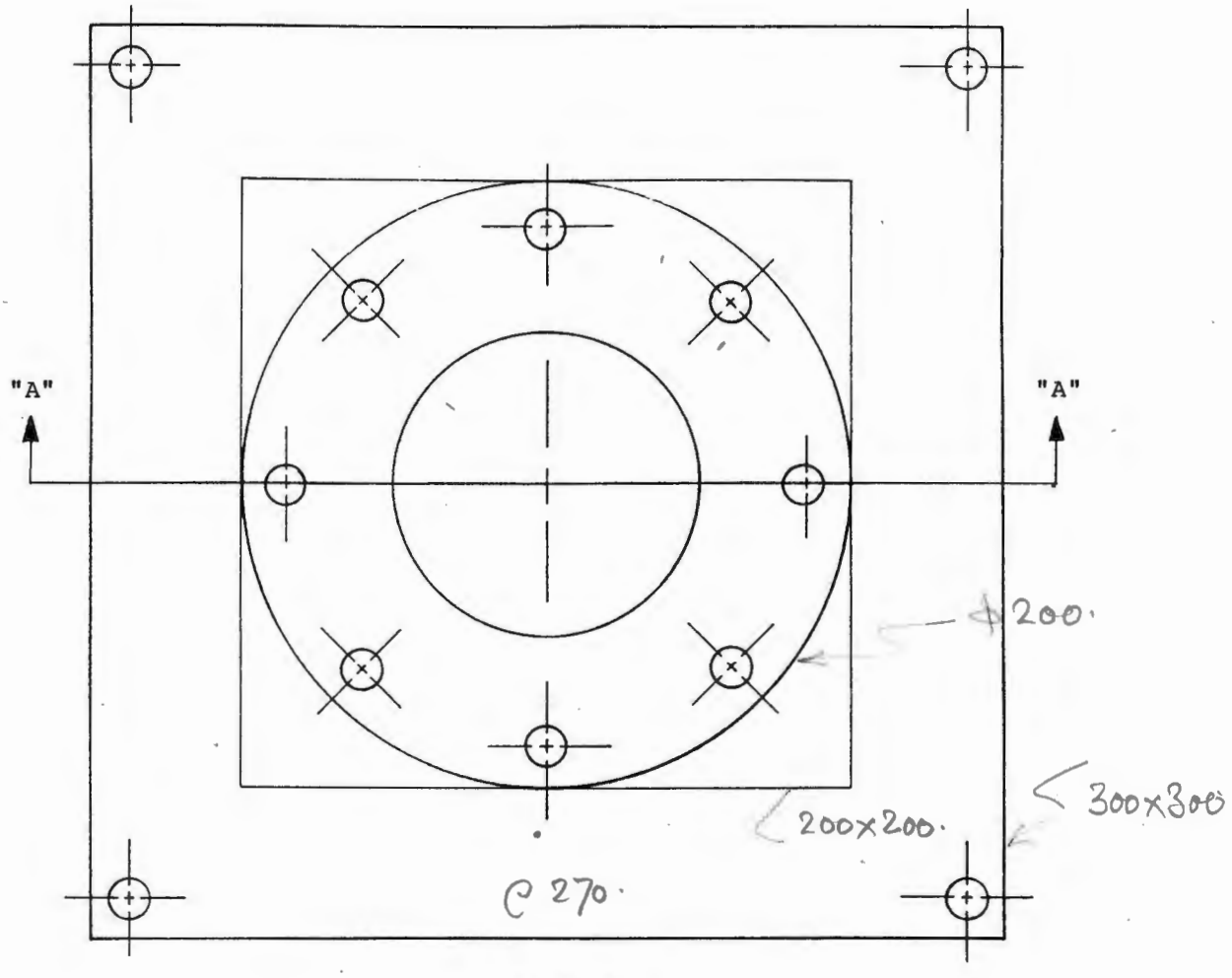

PLAN VIEW

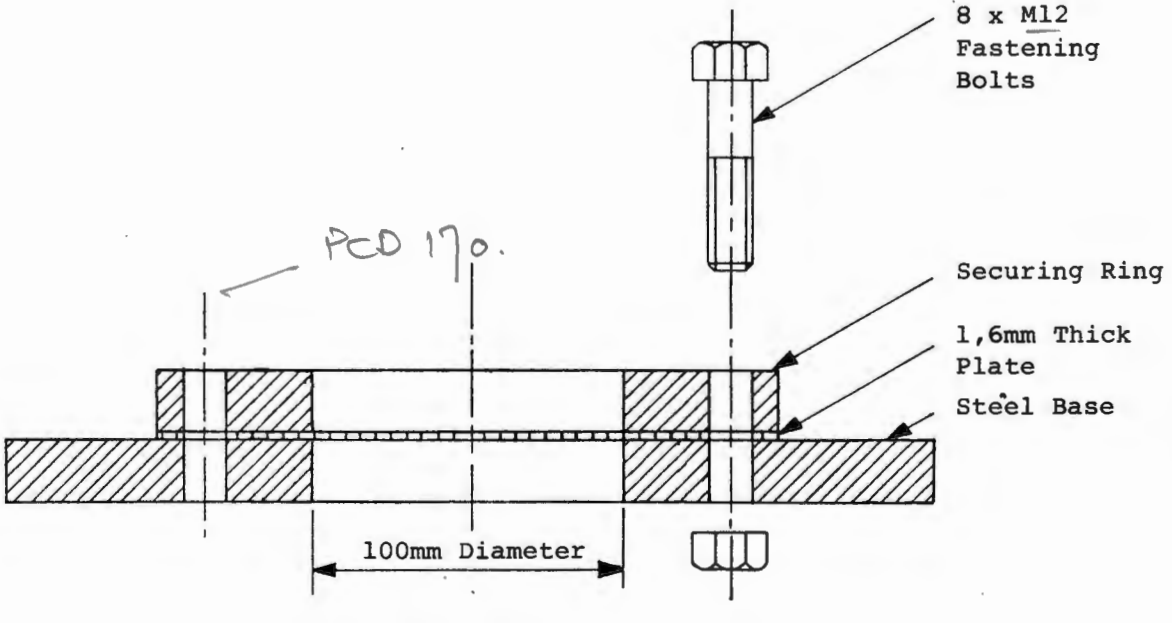

SECTION AA

FIGURE 2.3 TEST PLATE AND CLAMPING DEVICE

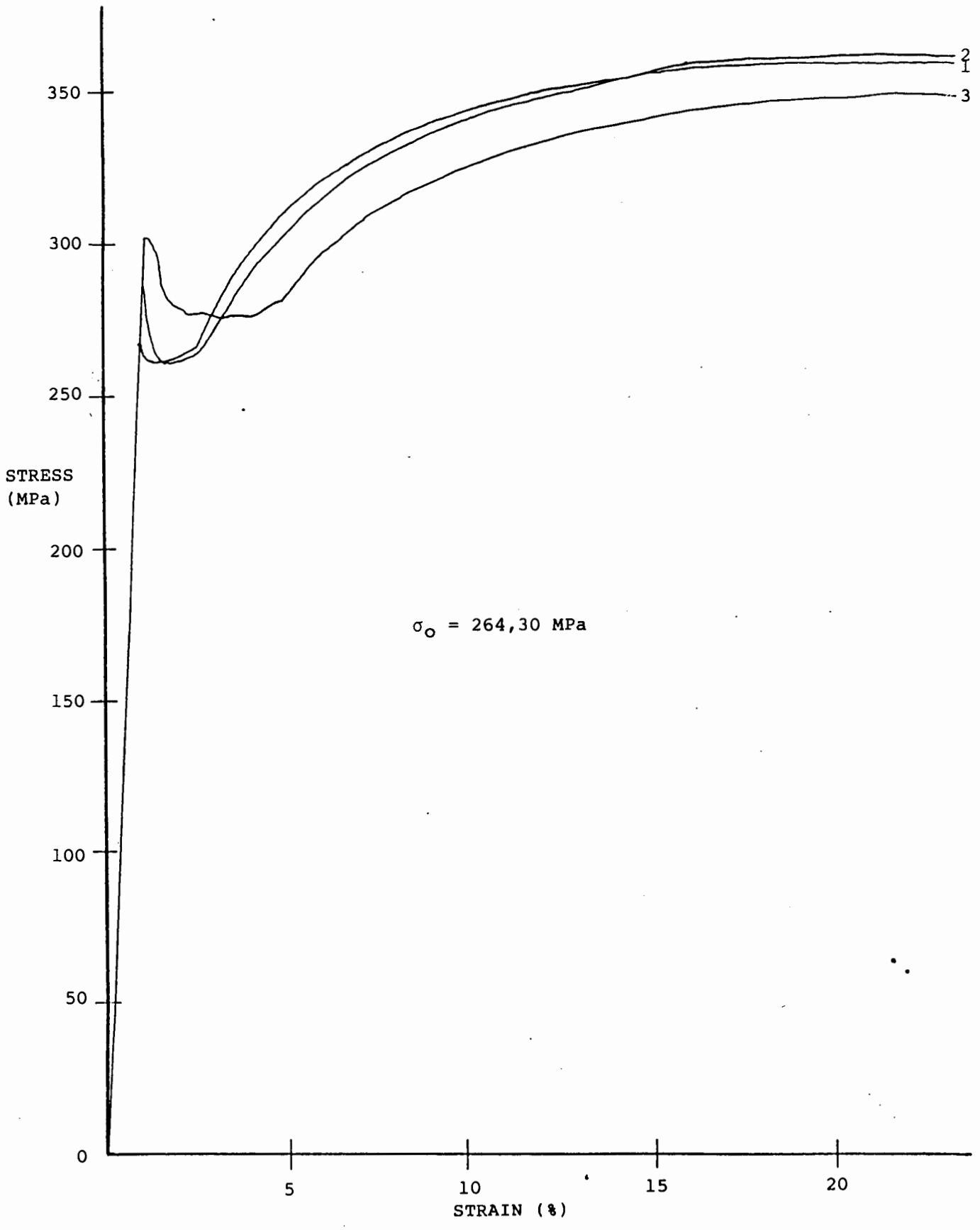

FIGURE 2.4a UNIAXIAL STRESS STRAIN TENSILE TEST FOR SHEET I

Strain Rates 1. $3{,}33 \times 10^{-4}$
2. $1{,}33 \times 10^{-3}$
3. $6{,}67 \times 10^{-3}$

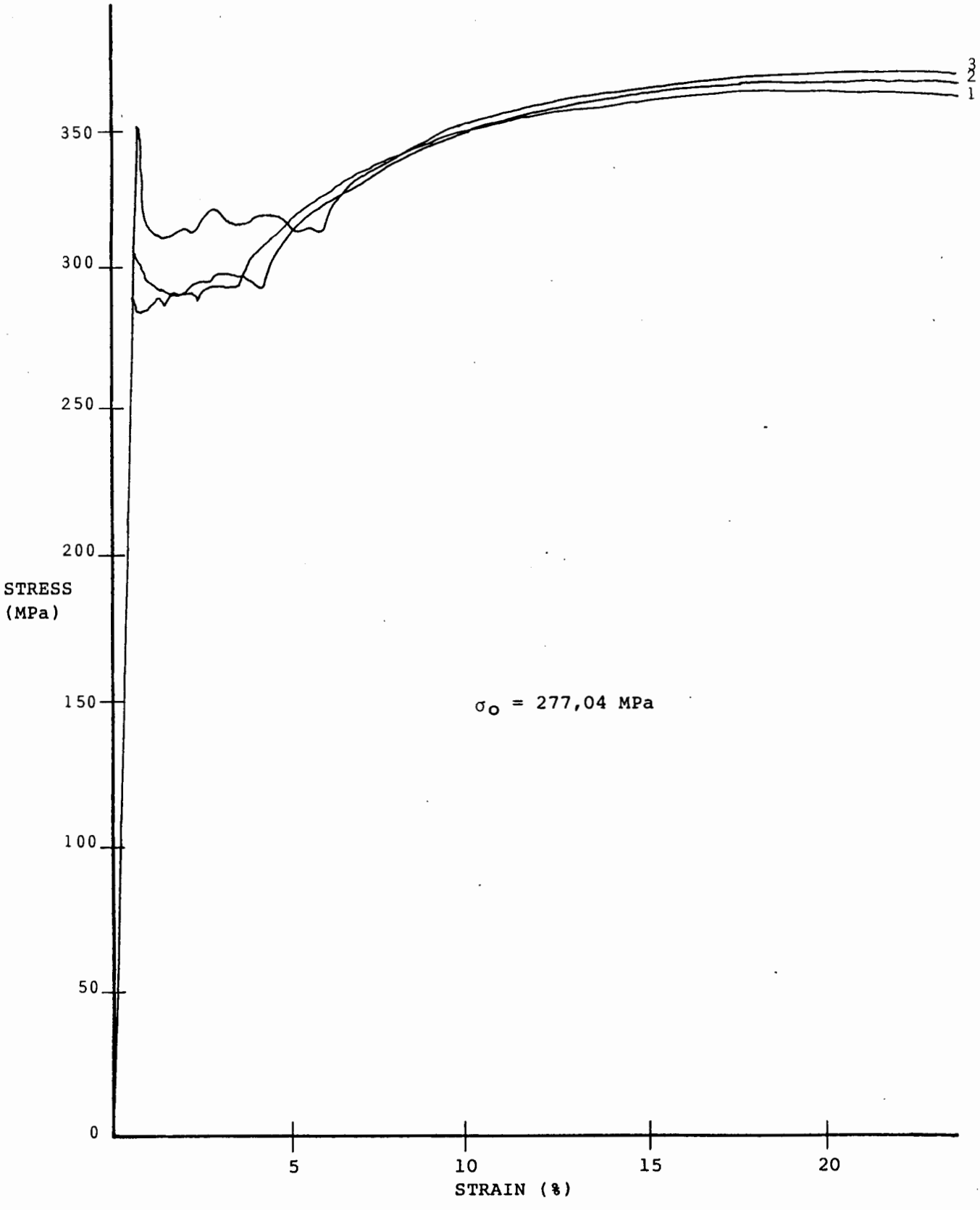

FIGURE 2.4b UNIAXIAL STRESS-STRAIN TENSILE TEST FOR SHEET II

Strain Rates 1. $3{,}33 \times 10^{-4}$
2. $1{,}33 \times 10^{-3}$
3. $6{,}67 \times 10^{-3}$

the Cowper-Symonds rigid viscoplastic constitutive equation

$$\frac{\sigma_o{}^1}{\sigma_o} = 1 + \left(\frac{\dot{\varepsilon}}{\dot{\varepsilon}_o}\right)^{1/n}$$

Where σ_o is the static yield stress, $\dot{\varepsilon}$ the uniaxial strain rate, σ_o^1 the dynamic yield stress while $\dot{\varepsilon}_o$ and n are material constants. Jones [14] reported that $\dot{\varepsilon}_o = 40\ sec^{-1}$ and n = 5 give reasonable agreement with the average of the available experimental data on mild steel given by Symonds in 1967.

The average static yield stress for the two sets of material are 264,30 MPa and 277,04 MPa. All the results for the tensile tests are given in Appendix A. The mild steel used is highly strain rate sensitive and shows considerable strain hardening during the experiments which result in a strain rate in excess of 7400 sec^{-1} calculated by using the dynamic and static yield stresses in the Cowper-Symonds equation (Appendix A). The determination of the dynamic yield stress can be seen in Section 3.3. The effect of strain hardening will be discussed in Section 3.3. Table 2.1 gives a summary of the test plate dimensions and mechanical properties.

TABLE 2.1 TEST PLATE DIMENSIONS AND MATERIAL PROPERTIES

Test Material	**Cold-Rolled Mild Steel**
Radius (R)	50mm
Thickness (t)	1,6mm
Density (ρ)	7850 $kg.m^{-3}$
$\dot{\varepsilon}_o$	40 sec^{-1}
n	5
Poisson's Ratio (ν)	0,33
Uniaxial Yield Stress	264,30 MPa --- Sheet I
	277,04 MPa --- Sheet II
Ultimate Tensile Stress	364,51 MPA --- Sheet I
	368,05 MPa --- Sheet II

The two different values given for the yield stress and the UTS correspond to the test material which was taken from two different sheets of cold-rolled mild steel. Although both the yield stress and UTS values are given, only the values for the yield stress are used.

2.3.3 Ballistic Pendulum

Fig 2.5 illustrates the experimental arrangement employed in the investigation reported here. The

ballistic pendulum consists of an I-beam suspended from the concrete slab ceiling of the 2,5m x 3,5m blasting room by means of four strands of spring steel wire. Each of the four stands have adjustable screws to enable the pendulum to be levelled. At one end of the pendulum is attached the experimental rig.

The rig includes two heavy steel plates which are used to rigidly clamp the test plate by means of eight fastening bolts, as well as a device for determining the velocity of the disc. The velocity of the metal disc necessitates some form of catching device which prevents the deformation of the disc during its deceleration. This is best performed by attaching a wooden box filled with an energy absorbent material to the experimental rig. At the other end of the pendulum is a fixture on which balancing masses can be placed. This ensures that each suspending wire carries approximately the same mass and that the impulse acts through the centroid of the pendulum. A pen for recording the pendulum oscillation on tracing paper is also attached at the back of the pendulum. The momentum imparted to a test specimen is related directly to the amplitude of the initial swing and this is recorded on the tracing paper.

The pendulum geometry is shown in Fig 2.6.

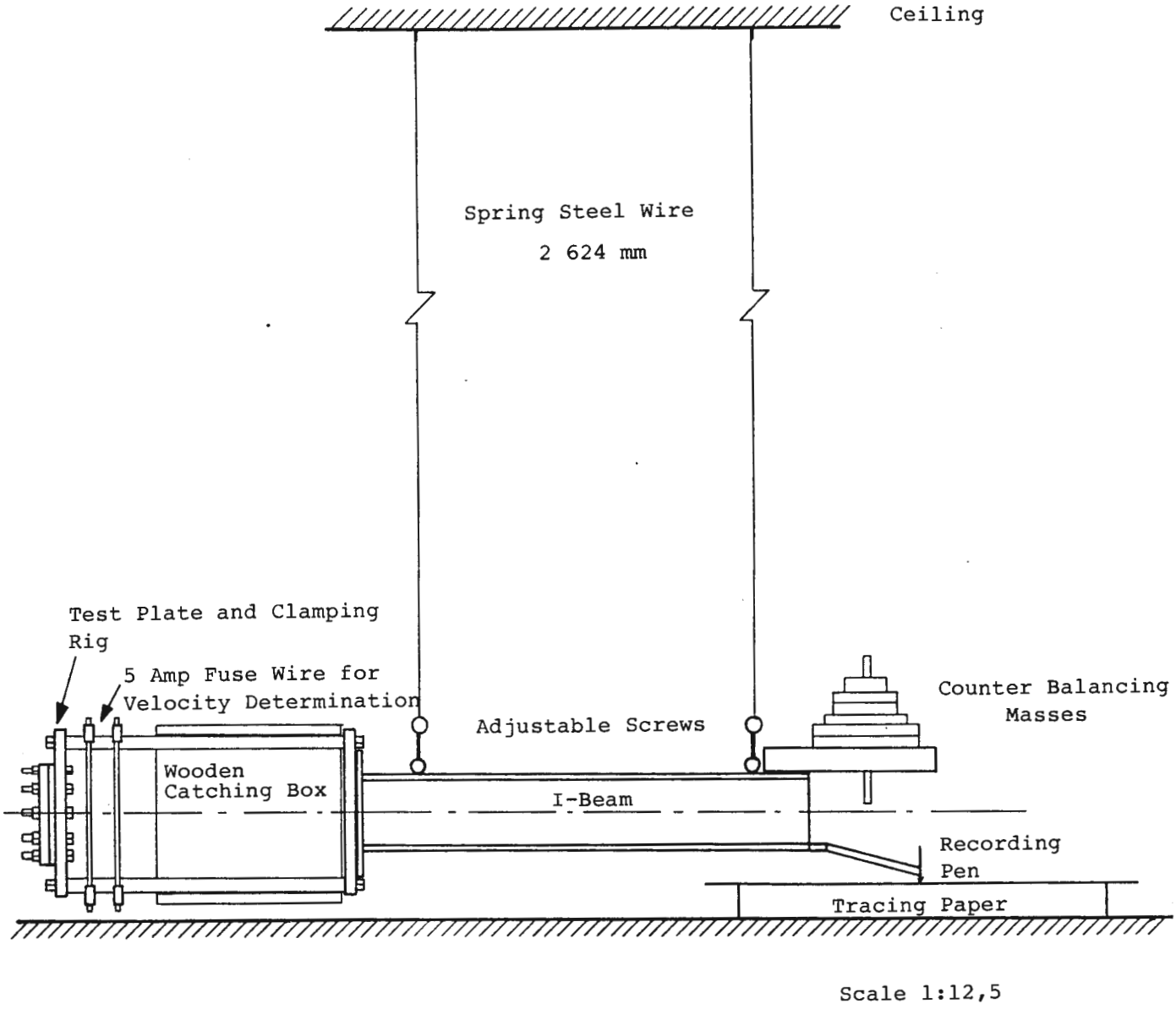

FIGURE 2.5 EXPERIMENTAL ARRANGEMENT

The linearised equation of motion of the pendulum, assuming viscous damping, is

$$\ddot{x} + 2\beta\dot{x} + w_n^2 x = 0 \qquad (2.1)$$

where

$$\beta = \frac{C}{2M}, \quad \omega_n = \frac{2\pi}{T} \text{ and } \omega_d = (\omega_n^2 - \beta^2)^{\frac{1}{2}}$$

and C is the damping coefficient, M is the total mass of the pendulum including the experimental rig, the balancing masses and explosives, and T is the natural period of the pendulum motion.

The solution of equation (2.1) is given by

$$x = \frac{(e^{-\beta t})\ \dot{x}_o \sin \omega_d t}{\omega_d} \qquad (2.2)$$

where $\dot{x}_o$ is the initial velocity of the pendulum.

Let x_1 be the horizontal displacement at $t = \frac{T}{4}$ and
$-x_2$ be the horizontal displacement at $t = \frac{3T}{4}$

Substituting into (2.2) gives

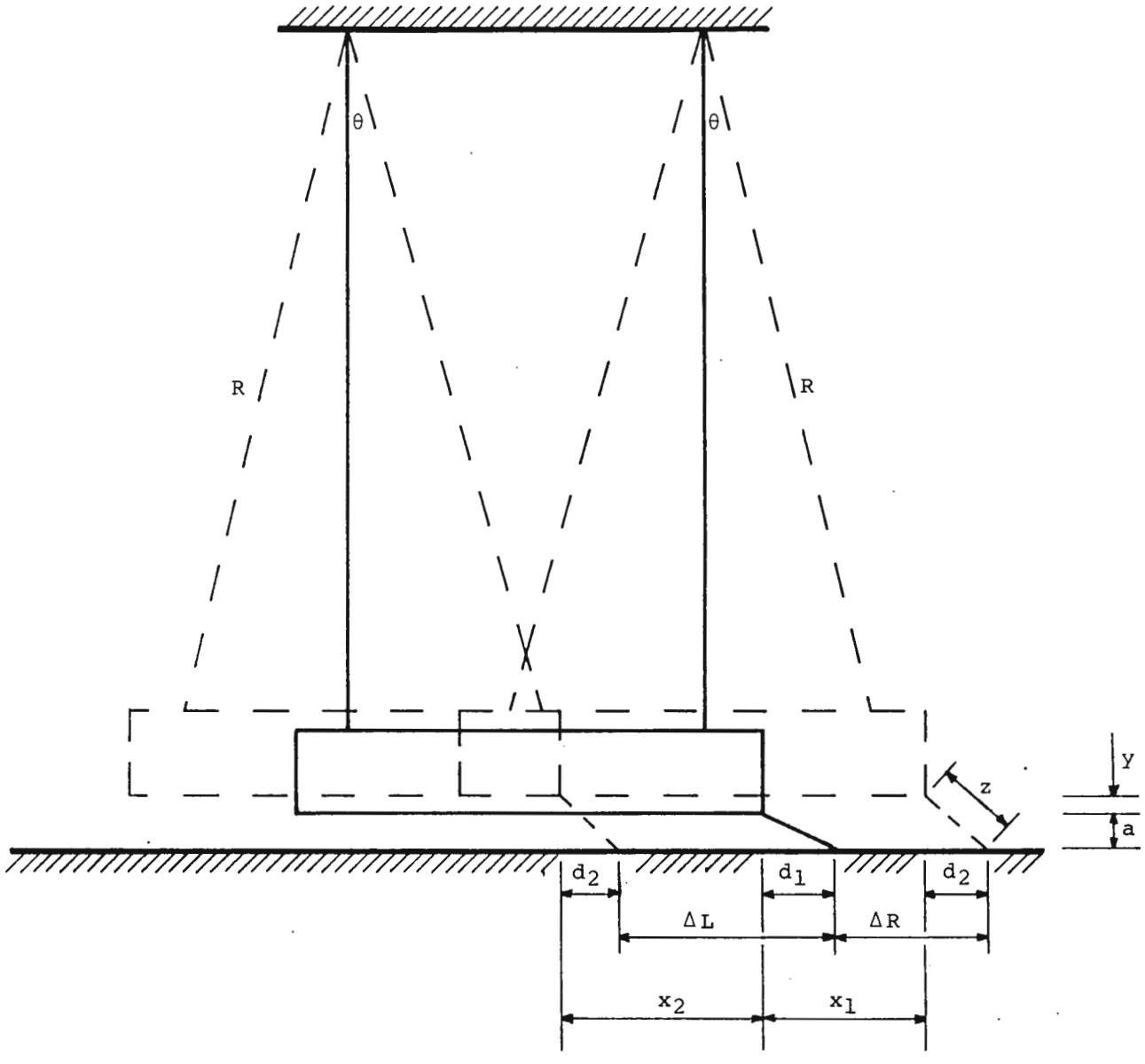

FIGURE 2.6 BALLISTIC PENDULUM GEOMETRY

$$x_1 = \frac{\dot{x}_o T}{2\pi} \; e^{-\frac{1}{4}\beta T} \tag{2.3}$$

$$x_2 = \frac{\dot{x}_o T}{2\pi} \; e^{-\frac{3}{4}\beta T} \tag{2.4}$$

Hence

$$\frac{x_1}{x_2} = e^{\frac{1}{2}\beta T}$$

which gives

$$\beta = \frac{2}{T} \ln \frac{x_1}{x_2} \tag{2.5}$$

and

$$\dot{x}_o = \frac{2\pi}{T} \; x_1 \; e^{\frac{1}{4}\beta T}$$

The impulse can therefore be found from

$$I = M\dot{x}_o \tag{2.6}$$

The period T is determined by taking the average of a number of measured pendulum oscillations with the mass being the same as that during testing. The damping constant, β, is calculated from equation (2.5) where

x_1 and x_2 are found from a number of pendulum oscillations in which the pendulum is held away from the vertical and released a number of times.

It will be noticed from observation of the pendulum geometry, Figure 2.6, that the distance moved by the pendulum, x_1, and that measured by the pendulum, ΔR, is not the same and this must be accounted for. By considering Figure 2.6 it is noticed that when the pendulum is stationary the horizontal distance from the end of the pendulum to the pen is given by

$$d_1 = (z^2 - a^2)^{\frac{1}{2}} \tag{2.7}$$

while at peak oscillations this distance decreases and is given by

$$d_2 = (z^2-(a + y)^2)^{\frac{1}{2}} \tag{2.8}$$

The small oscillations of the pendulum during testing ensure that θ is very small and therefore the assumption can be made that

$$x_1 \simeq R\,\theta \text{ and } y \simeq \frac{R\theta^2}{2}$$

Therefore

$$y = \frac{x_1^{\,2}}{2R} \tag{2.9}$$

and $$d_2 = (z^2 - (a + \frac{x_1^2}{2R})^2)^{\frac{1}{2}} \qquad (2.10)$$

From Figure 2.6

$$x_1 = \Delta R + d_1 - d_2$$

and $$x_2 = \Delta L - d_1 + d_2$$

Substituting for d_1 and d_2 gives

$$x_1 = \Delta R + (z^2 - a^2)^{\frac{1}{2}} - [z^2 - (a + \frac{x_1^2}{2R})^2]^{\frac{1}{2}} \qquad (2.11)$$

and $$x_2 = \Delta L - (z^2 - a^2)^{\frac{1}{2}} + [z^2 - (a + \frac{x_1^2}{2R})^2]^{\frac{1}{2}} \qquad (2.12)$$

ΔL, ΔR, Z, a and R are measured and therefore x_1 and x_2 can be calculated . Table 2.2 gives all the constants of the ballistic pendulum during the experiments.

TABLE 2.2 BALLISTIC PENDULUM DETAILS

R	-	2 624 mm	Mass of I-beam	-	22,0 kg
Z	-	160 mm	Mass of Test Rig	-	39,73 kg
a	-	46 mm	Mass of Counter Balance	-	27,0 kg
T	-	3,22 seconds			
β	-	0,0235	Typical pen stroke ie. ΔR 25 - 290 mm		
M	-	88,73 kg			

2.3.4 Explosive Material, Mass and Geometry

Metabal sheet explosive was used throughout the experimental work. The plastic explosive was supplied with the following specifications, an average thickness of 3,2mm, a density of 1,47 $g.cm^{-3}$ and a detonation velocity of 6500 - 7500 $m.s^{-1}$. The speed of detonation being sufficiently large to assume that an ideal impulse is simultaneously applied over the whole plate.

The two ring configuration used by Nurick [3] is also used during this study as it enables comparisons relating impulse and mass of explosive to be made between the two sets of experimental results.

In all the experiments the Metabel is arranged as shown in Fig 2.7. The two rings are interconnected by a cross leader, which in turn is connected by a main leader at the centre to a shielded detonator.

In all the cases the explosive is placed on a 14mm thick polystyrene pad with the same diameter as the circular plate. This attenuator is used to reduce the high peak pressure in the wave entering the plate, provide a uniform impulse and prevent spallation of the specimen.

The advantages of being able to measure the impulse for each individual test from the deflection of the pendulum, avoid the necessity of :

a) a separate series of calibration tests
b) the possible variation in the specified specific impulse of the explosive
c) the variation that might occur because of factors such as variable plate material, geometry and boundary conditions.

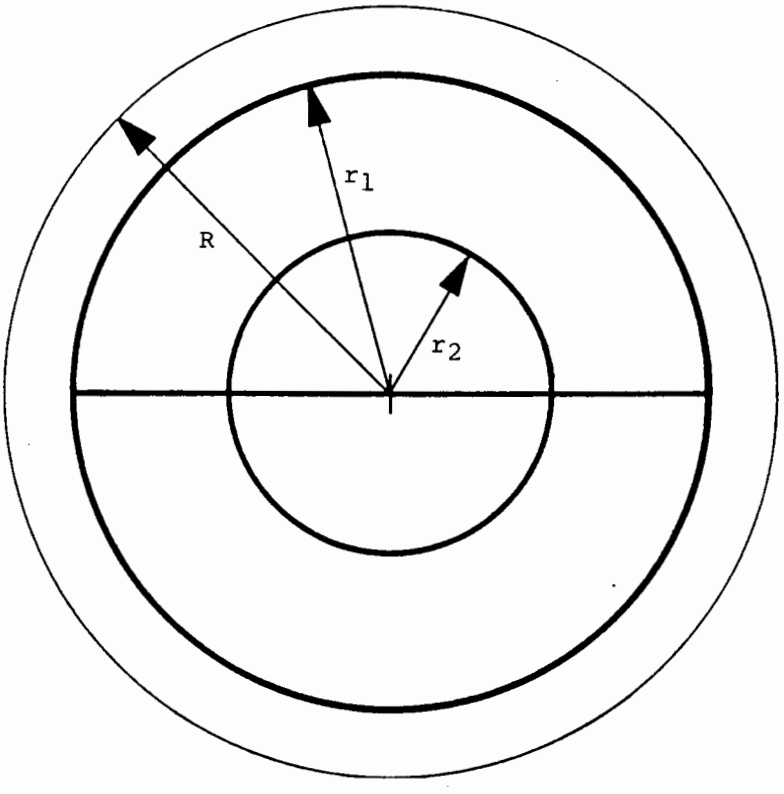

$r_1 = 0{,}82\ R$

$r_2 = 0{,}41\ R$

Total Mass of Explosive = M

Mass of Leader and detonator connector = 2 g

therefore $m_1 = \frac{1}{3}(M-2)$ g

$m_2 = \frac{2}{3}(M-2)$ g

FIGURE 2.7 EXPLOSIVE CONFIGURATION

The Metabel used in the experiments in this investigation has a very varied make-up. It is thus important to overcome these factors. This is done so by being able to measure the individual impulses for each test.

Figure 2.8 shows a plot of the mass of explosives versus the impulse. Although the correlation according to a least squares lines is good (r = 0,977) it can be seen that in some cases the variations are quite large.

In previous experimentation by Nurick [3] using the same type of Metabel explosive and the corresponding 2-ring explosive configuration during testing on the deformation of clamped circular plates, it was found that a plot of impulse against mass of explosive gave the following least squares line.

$$I = 2,18M - 4,4 \quad \text{with} \quad r = 0,96$$

In the present study the least squares line determined is

$$I = 1,96M + 5,28 \quad \text{with} \quad r = 0,977$$

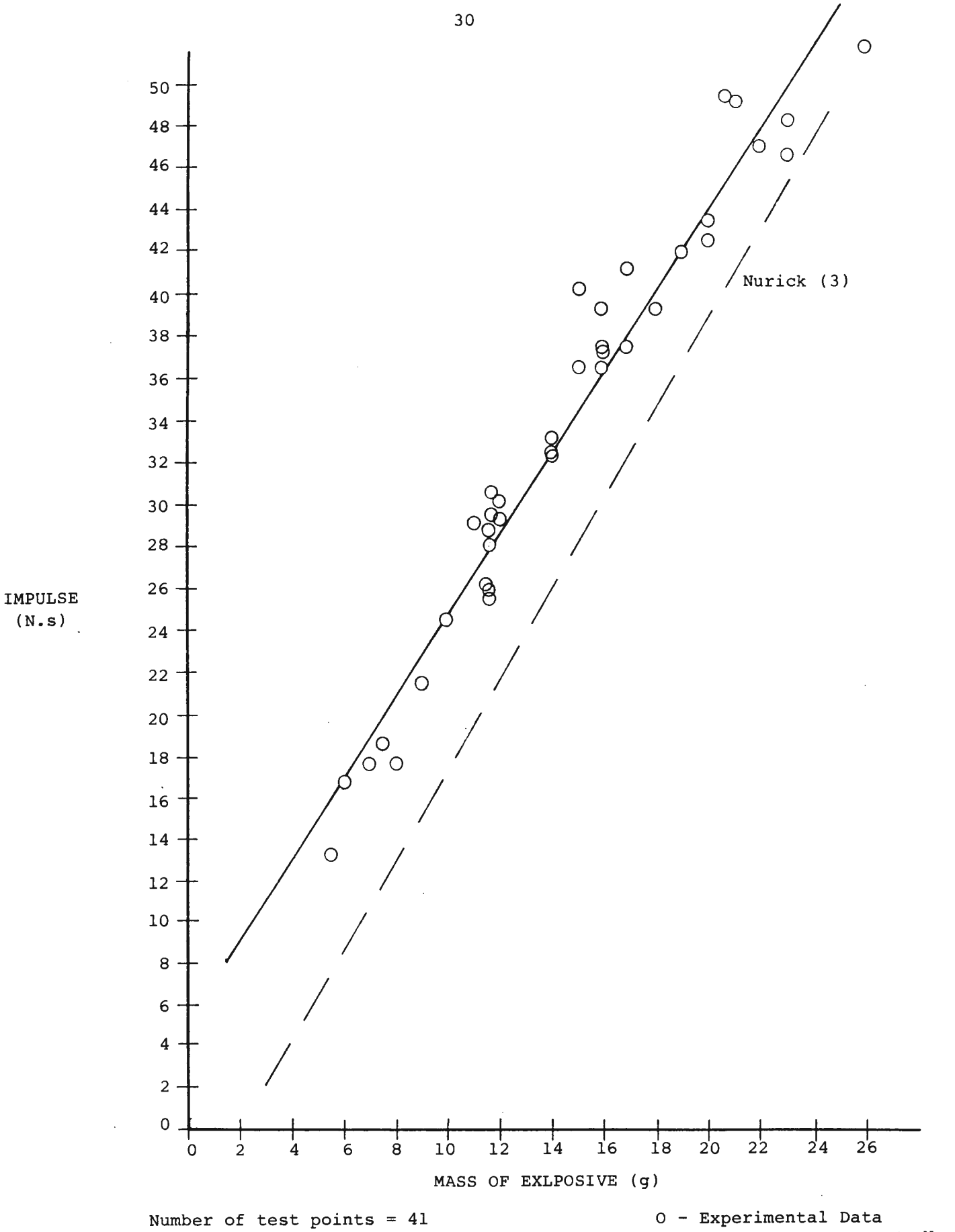

FIGURE 2.8 GRAPH OF MASS OF EXPLOSIVE vs IMPULSE

Figure 2.8 shows that the slopes of the equations are similar but the intercept points are different. The only explanation that can be given to explain these differences is that each set of tests were performed using different batches of Metabel and it could be that the constitutive components varied slightly between these two batches, thereby giving slightly different results. It is therefore once again seen how important it is to be able to measure the impulse from each individual test and not rely on separate calibration tests performed to determine the impulse per unit mass of explosive.

2.3.5 Determination of Plate Velocity after Tearing

The velocity of the disc is measured when two thin wires are broken in succession. Two five amp fuse wires are stretched, a known distance apart, across the intended path of the metal disc. Each wire is connected to a resister which is in turn connected to a nine volt power supply unit (Figure 2.9). When the wires are broken a voltage can be measured across each of the points. The voltage step is recorded in each case on a dual channel digital memoryscope. The oscilloscope is triggered by the breaking of the first wire which is connected to channel 1, when the second

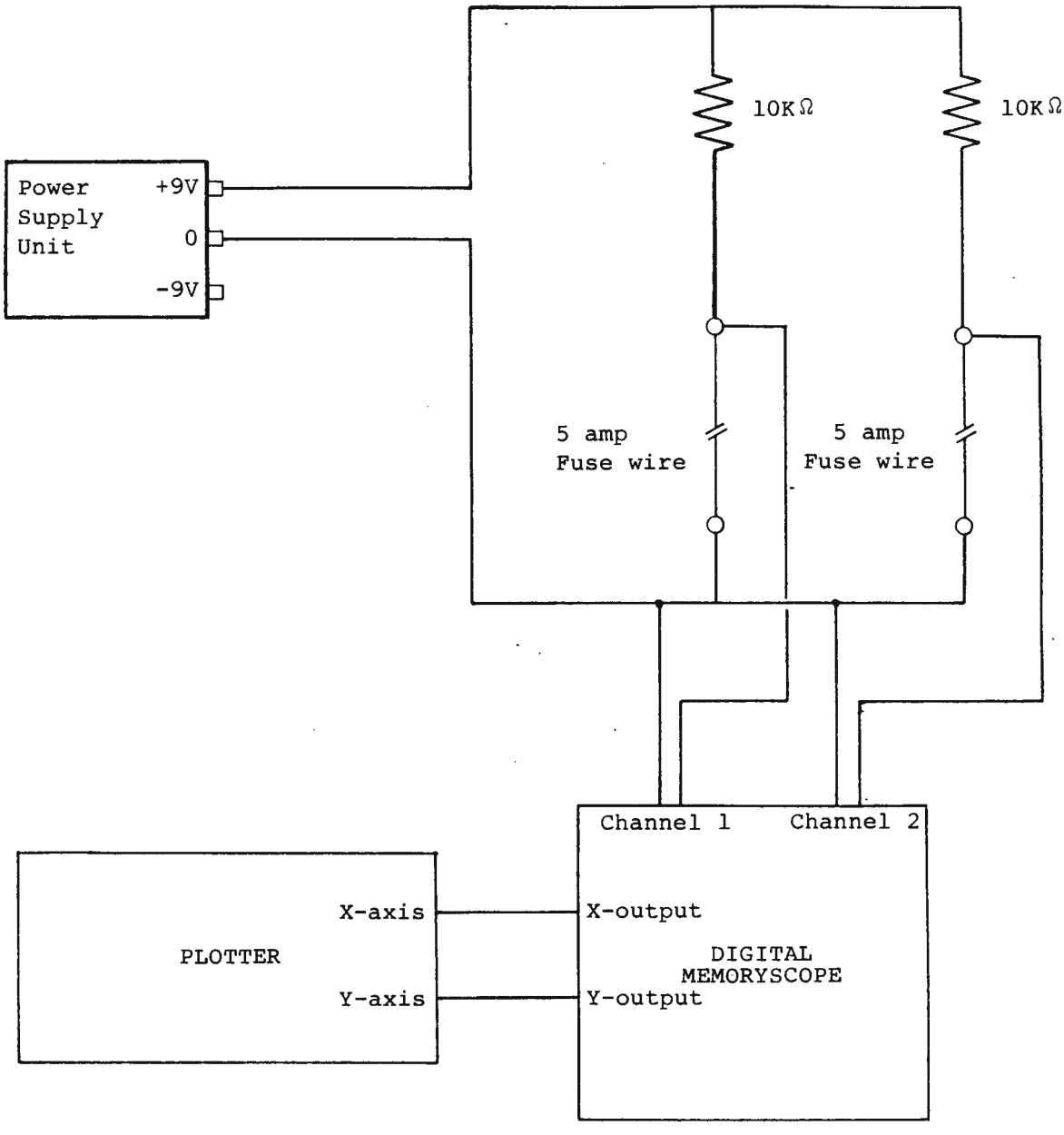

FIGURE 2.9 ELECTRICAL CIRCUIT FOR VELOCITY MEASUREMENT

wire is broken a second step function is recorded on the screen (channel 2). The time between the two changes in voltage can be accurately measured and the velocity of the disc can therefore be determined by knowing the distance between the fuse wires. The x and y outputs from the oscilloscope are connected to a plotter and the image on the screen in its original or expanded form can be recorded on graph paper.

2.4 CIRCULAR DISC ENTRAPMENT

In order for work to be done on the transition from the mode II to the mode III type of failures, very large impulsive forces, need to be imposed on the circular plate. This means that once complete tearing has taken place the velocity of the circular disc attains values in the range of 100-425m.s^{-1}. The shape of the deformation of the plate before tearing must be preserved and it is therefore necessary to stop the disc, and avoid any further deformation, over a distance of approximately four hundred millimetres. The small distance allowed to stop the disc is due to the nature of the experimental rig (Figure 2.5) and the size of the blasting room.

A wooden catching box (Figure 2.5) is attached to the test rig and stuffed with a variety of different materials. High density foam rubber and polystyrene were both packed tightly in the box but proved unsatisfactory and did not have the required decelerating effect on the disc, which after recovery from the box was deformed to such an extent as to make the measurement of the mid-point deflection and shape of deformation impossible.

It was found that by packing the catching box with aluminium filings (produced by the turning of aluminium on a lathe), the disc could be caught with the original shape being preserved.

2.5 TEST RESULTS

2.5.1 Experimental Reliability

Once the initial preliminary tests had been performed to obtain a basic idea of the nature of the work and after the experimental rig and ballistic pendulum had been modified and adjusted to give the desired readings, a total of 45 tests are conducted over a period of 8 working days of which 40 tests are performed over 7 days. The remaining 5 tests are conducted approximately one month later thereby showing that good repeatability is possible.

The experiments show an eighty percent success rate with 36 of the tests being completed in the following respect.

a) The explosive detonates correctly.
b) The initial deflection of the pendulum is recorded.
c) In those tests involving complete tearing the velocity of the circular disc is recorded.
d) There is little deformation in the catching box which enables the mid-point deflection to be measured.

The following problems are encountered in the remaining nine tests:

a) In one test there is incomplete detonation of the explosive.
b) In two tests there is a problem in the measurement of the pendulum movement. The pen fell off in one instance and in the other the tracing paper came loose.
c) In one test the electrical plug of the oscilloscope fell out of the wall during the explosion.
d) In three tests the metal disc did not come out straight and is either deformed to such an extent to prevent accurate deformations to be measured or

else both wires are not broken and therefore no velocity measurements could be made.

e) Reasons for unsuccessful tests could not be determined in two cases.

Apart from the last problem the previous four are typical of those associated with this type of experimentation and can be expected. The fourth problem only occurs when the tests are performed in the transition phase from partial tearing to complete tearing around the circumference of the circular plate, and is possibly associated with the plate material not being entirely homogeneous around the circumference.

2.5.2 **Test Readings**

2.5.2.1 Impulse

The initial deflection of the pendulum is measured and the Impulse determined from equation (2.6) in section 2.3.3.

2.5.2.2 Velocity of Circular Disc

In those tests involving complete tearing the time to travel the distance between the two 'break' wires is

recorded on the oscilloscope and the velocity is therefore determined. Typical oscilloscope outputs are shown in Figures 2.10 (a, b, c, d).

2.5.2.3 Measured Deflection

The final mid-point deflection is measured using two methods. A height vernier enables an accurate determination of the central height but proves inaccurate in determining the deformed shape along a particular cross-section. The second method involves the use of a reflex metrograph. This technique involves the digitising of approximately three hundred points on each plate, these are then interpolated and plotted. Contour paths and three-dimensional images are produced for a number of test plates and from the contour paths the deformed shape across selected cross-sections can be shown. Typical contour plots of deformed plates are shown in Figures 2.11 (a, b, c, d, e, f) while the three-dimensional plots are shown in Figures 2.12 (a, b, c).

2.5.2.4 Test Results of Uniaxial Yield Tests

These are shown in Figure 2.4 with more detailed results given in Appendix A.

2.5.2.5 Table of Test Data

Table 2.3 lists the test readings with the mass of explosive, corresponding impulse, Measured Mid-Point Deflection, Deflection-Thickness Ratio and where applicable the velocity of the circular disc being represented.

With the exception of the first test reading the data is listed in order of increasing mass of explosive. The values measured for the first test listed are those measured after incomplete detonation of the explosive charge. This test result is not used when plotting the graph in Figure 2.8 but is used in all other respects.

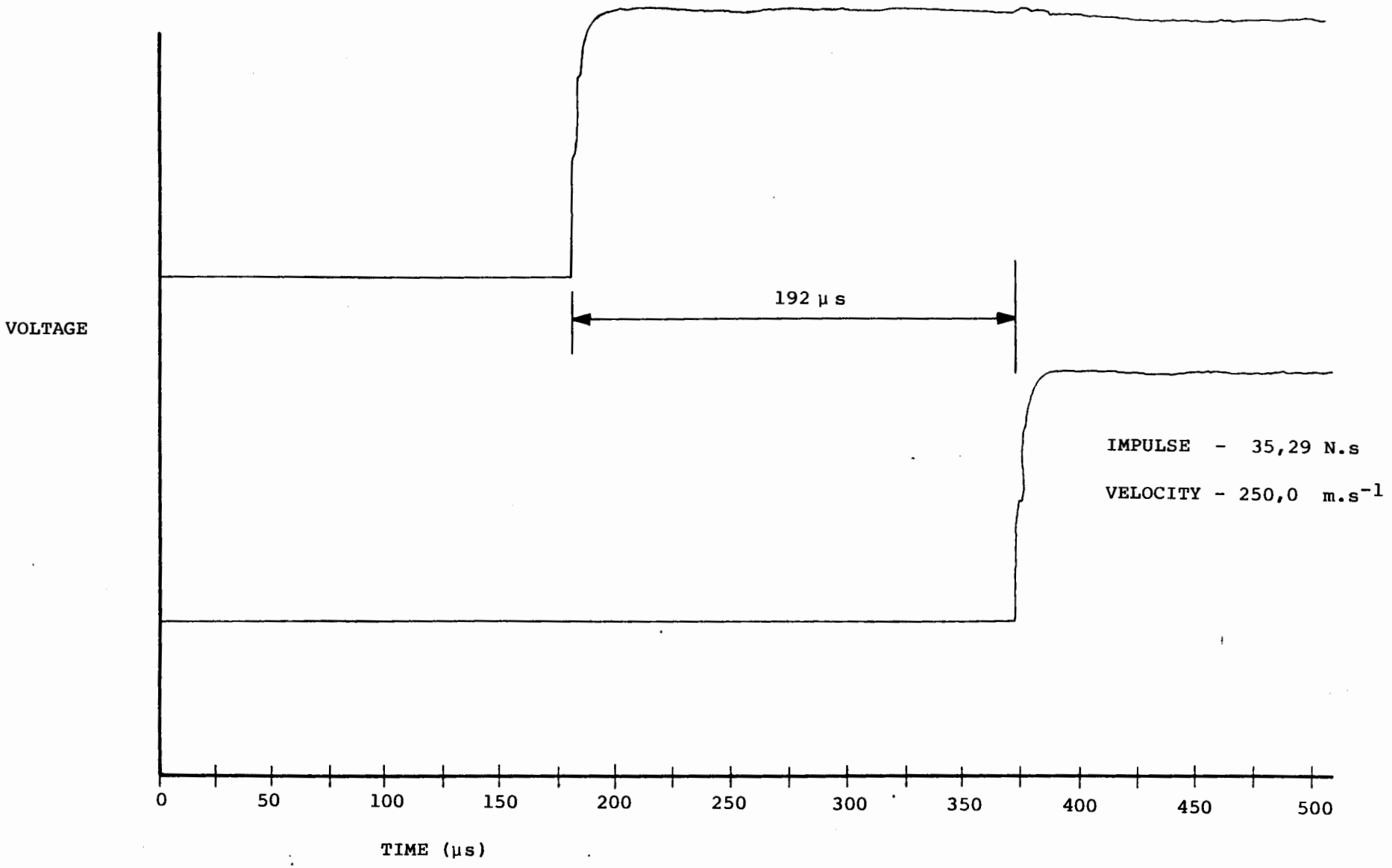

FIGURE 2.10a TYPICAL OSCILLISCOPE TIME MEASUREMENT TEST NO 250901

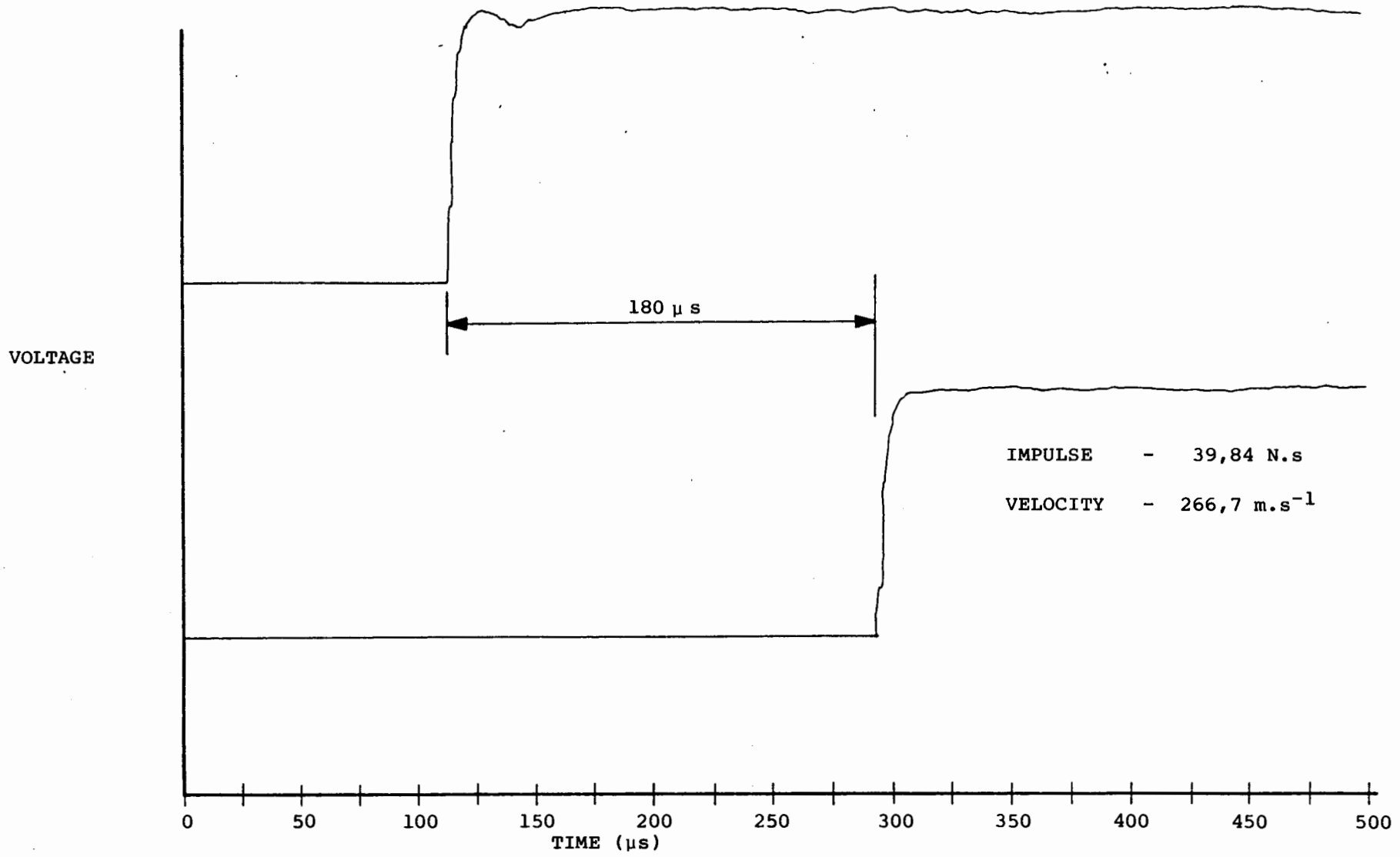

FIGURE 2.10b TYPICAL OSCILLISCOPE TIME MEASUREMENT TEST NO 250903

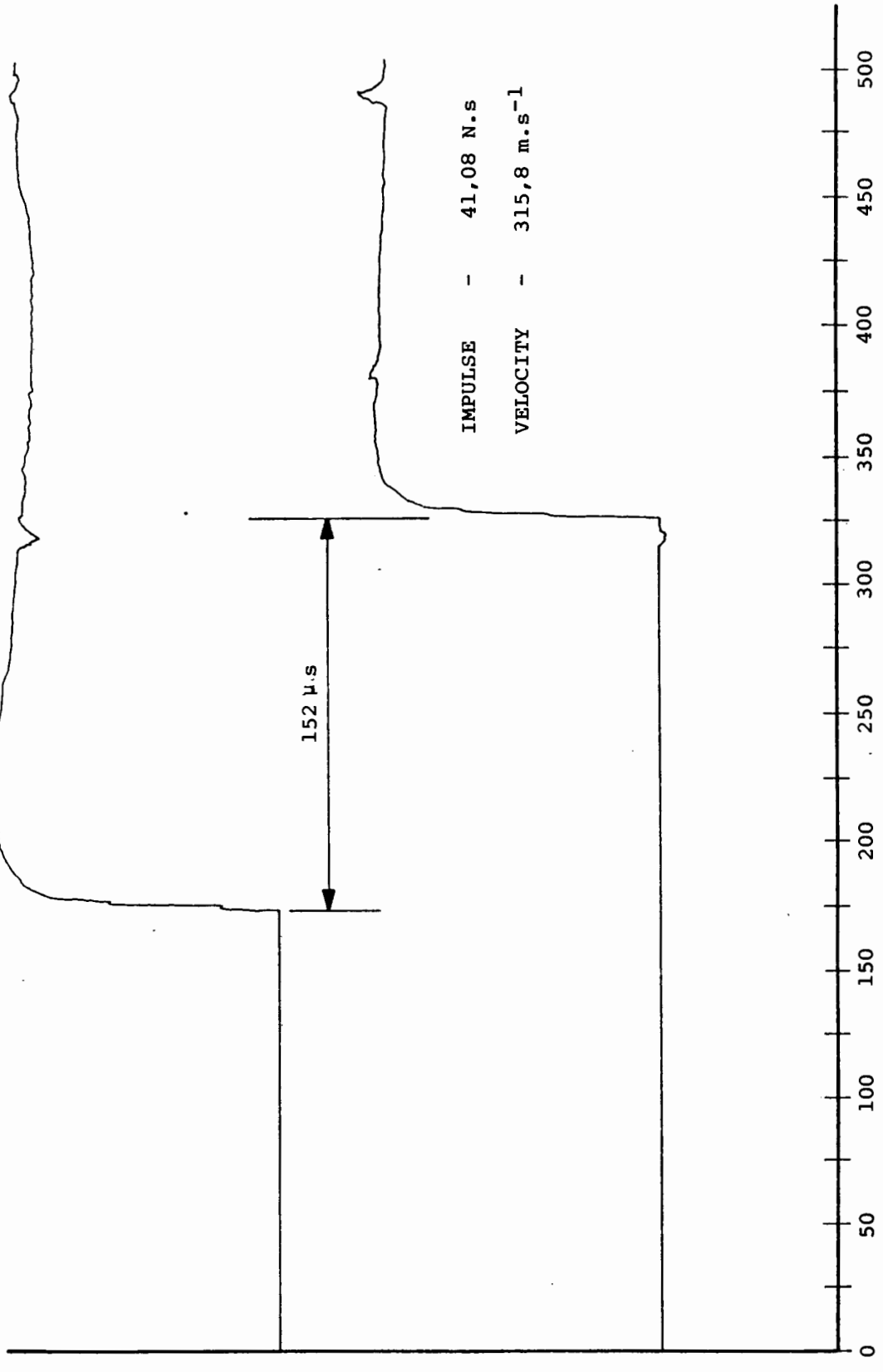

FIGURE 2.10c TYPICAL OSCILLISCOPE TIME MEASUREMENT TEST NO 250906

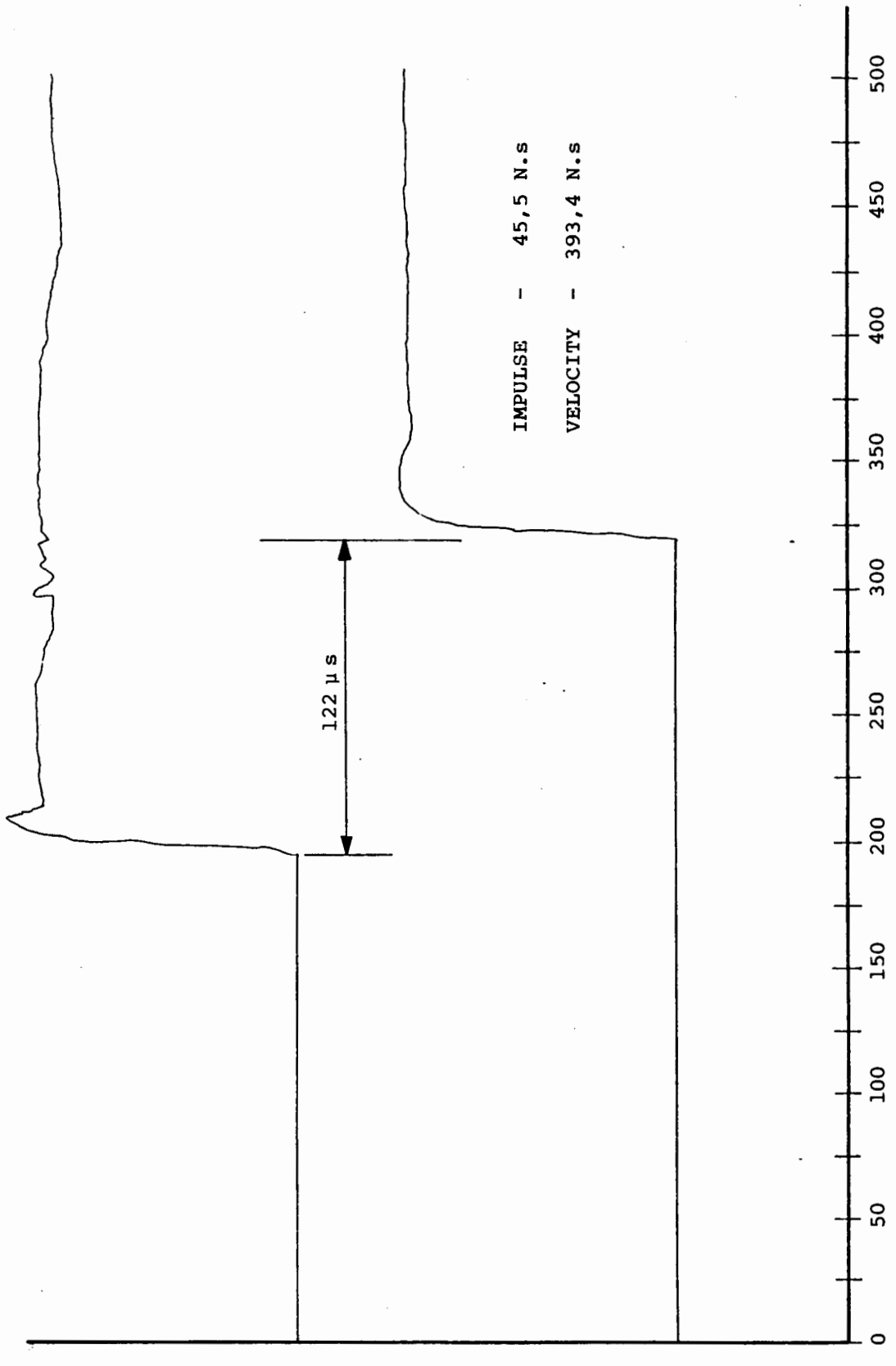

FIGURE 2.10d TYPICAL OSCILLISCOPE TIME MEASUREMENT TEST NO 270903

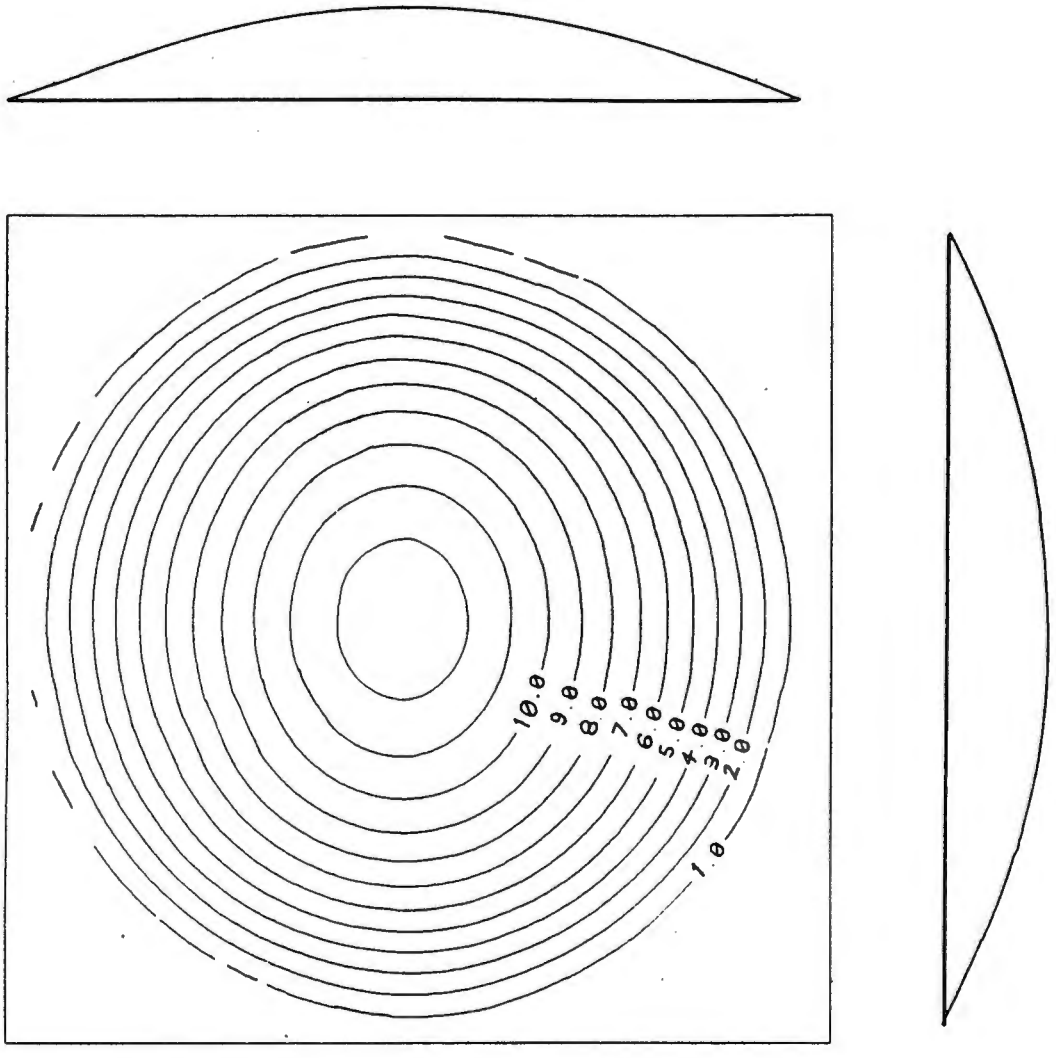

Test No 041006 (Deformation only, no tearing)

Impulse - 13,28 N.s
Mid-point Deflection - 12,5 mm

FIGURE 2.11a CONTOUR PLOT AND DEFORMATION PROFILES OF A DEFORMED PLATE

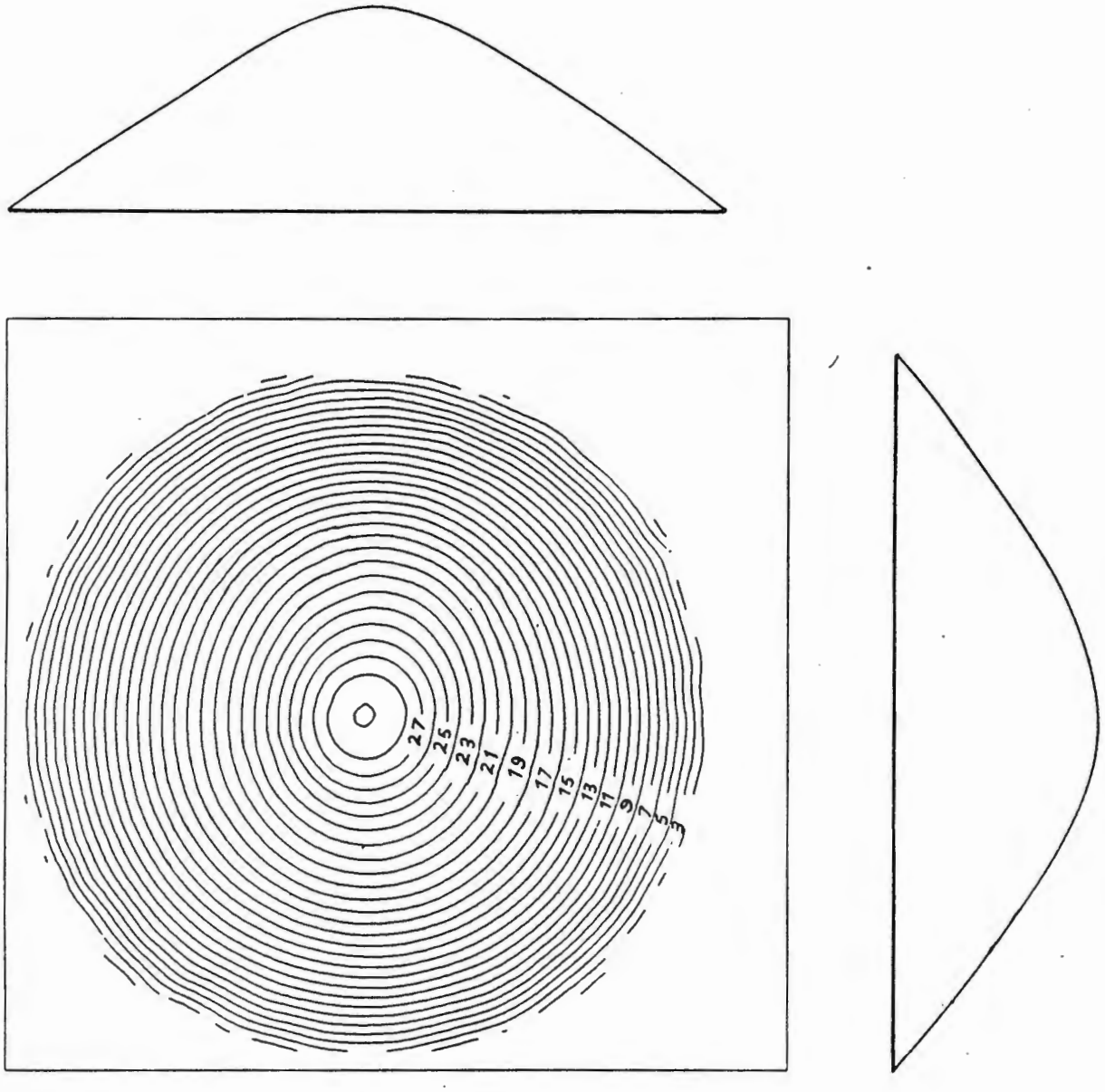

Test No 051005 (Deformation with signs of tearing along 5% of the circumference)

Impulse - 26,17 N.s
Mid-point Deflection - 26,2 mm

FIGURE 2.11b CONTOUR PLOT AND DEFORMATION PROFILES OF A DEFORMED PLATE

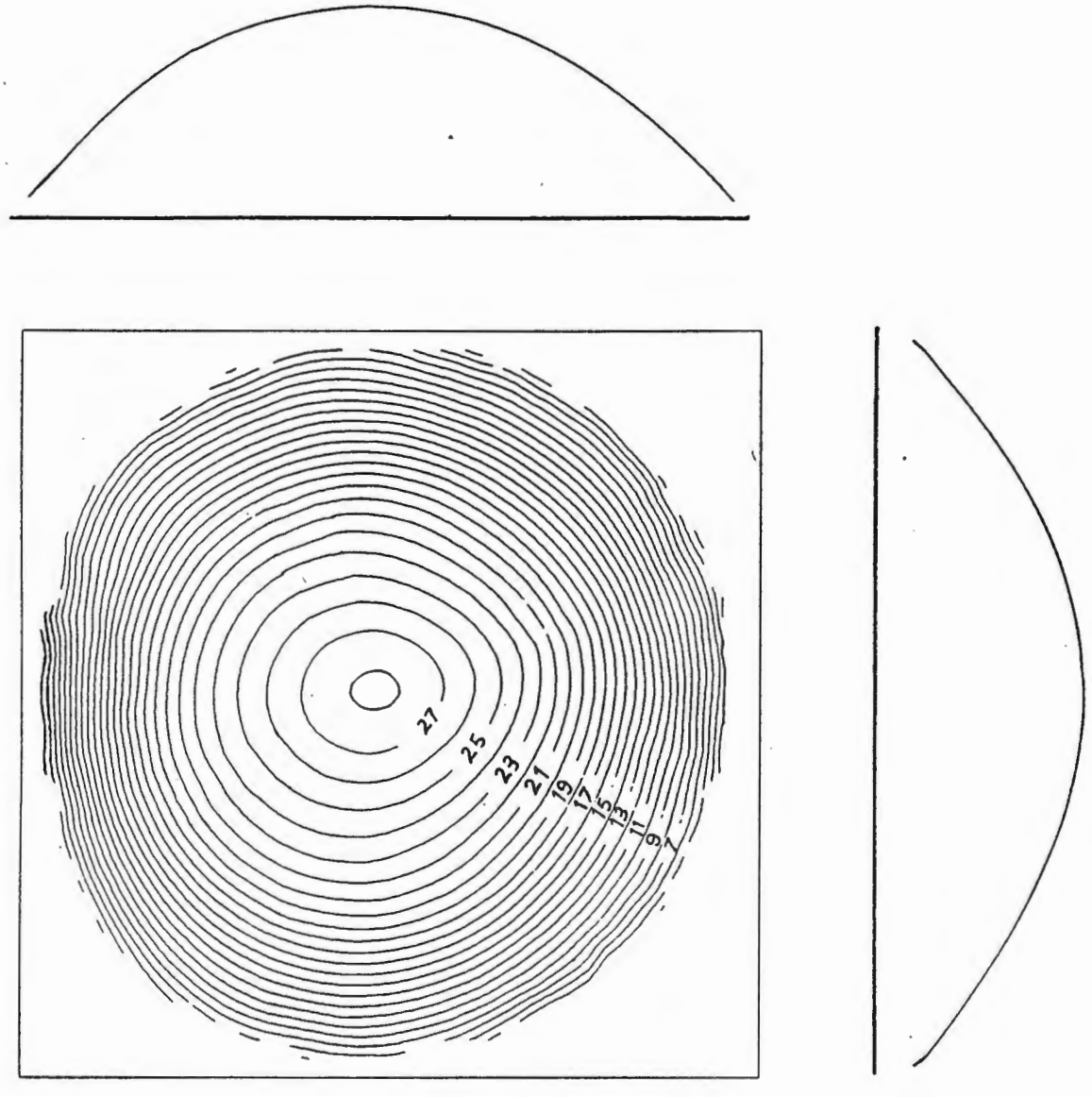

Test No 051001 (Complete tearing, 100%)

Impulse - 30,31 N.s
Mid-point Deflection - 24,1 mm (4mm is the zero on the contour plot)

FIGURE 2.11c CONTOUR PLOT AND DEFORMATION PROFILES OF A DEFORMED PLATE

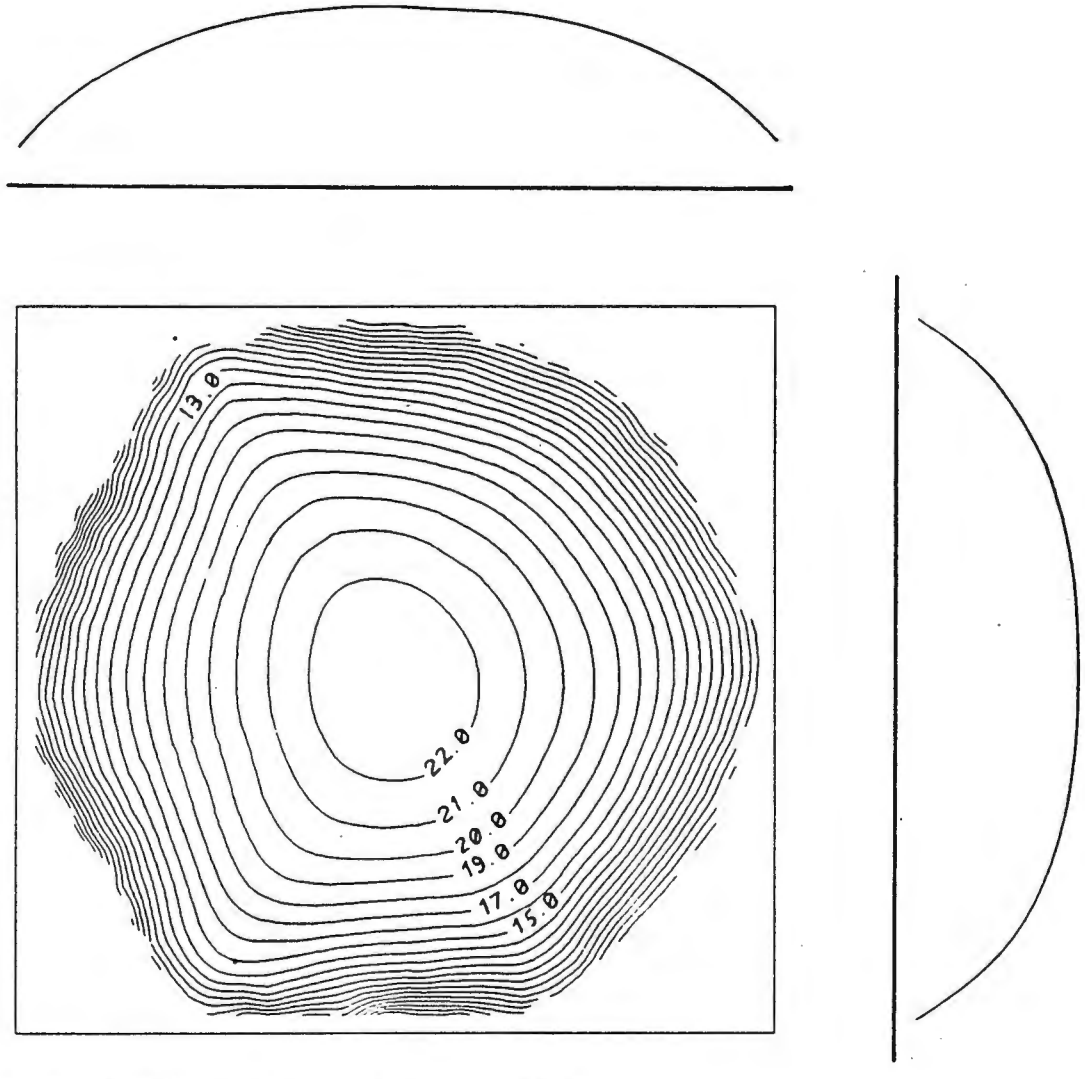

Test No 250902 (Complete tearing, 100%)

Impulse - 37,57 N.s
Mid-point Deflection - 20,6 mm (2mm is taken as the zero line on the contour plot)

FIGURE 2.11d CONTOUR PLOT AND DEFORMATION PROFILES OF A DEFORMED PLATE

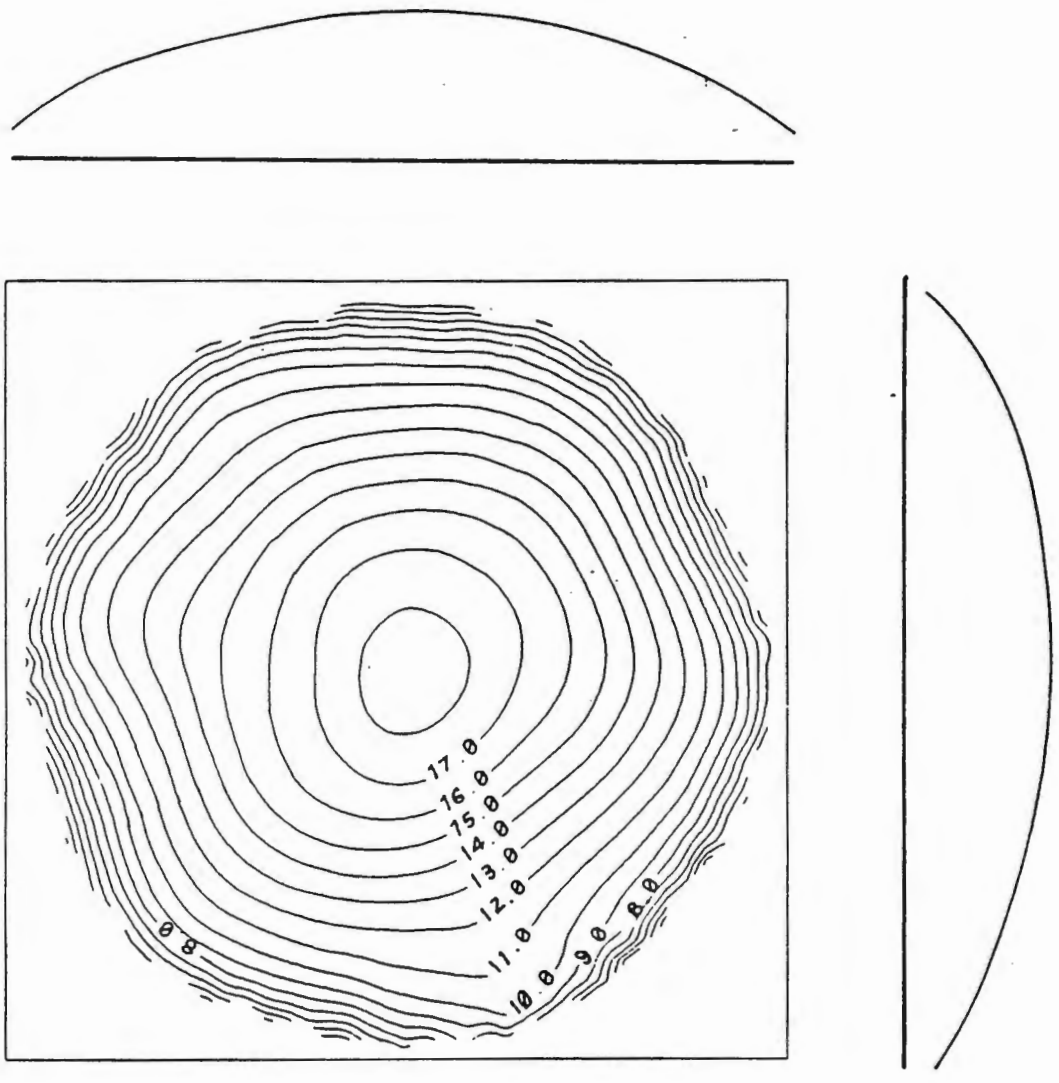

Test No 061001 (Complete tearing, 100%)

Impulse - 39,56 N.s
Mid-point Deflection - 16,3 mm (2mm is taken as zero on the contour plot)

FIGURE 2.11e CONTOUR PLOT AND DEFORMATION PROFILES OF A DEFORMED PLATE

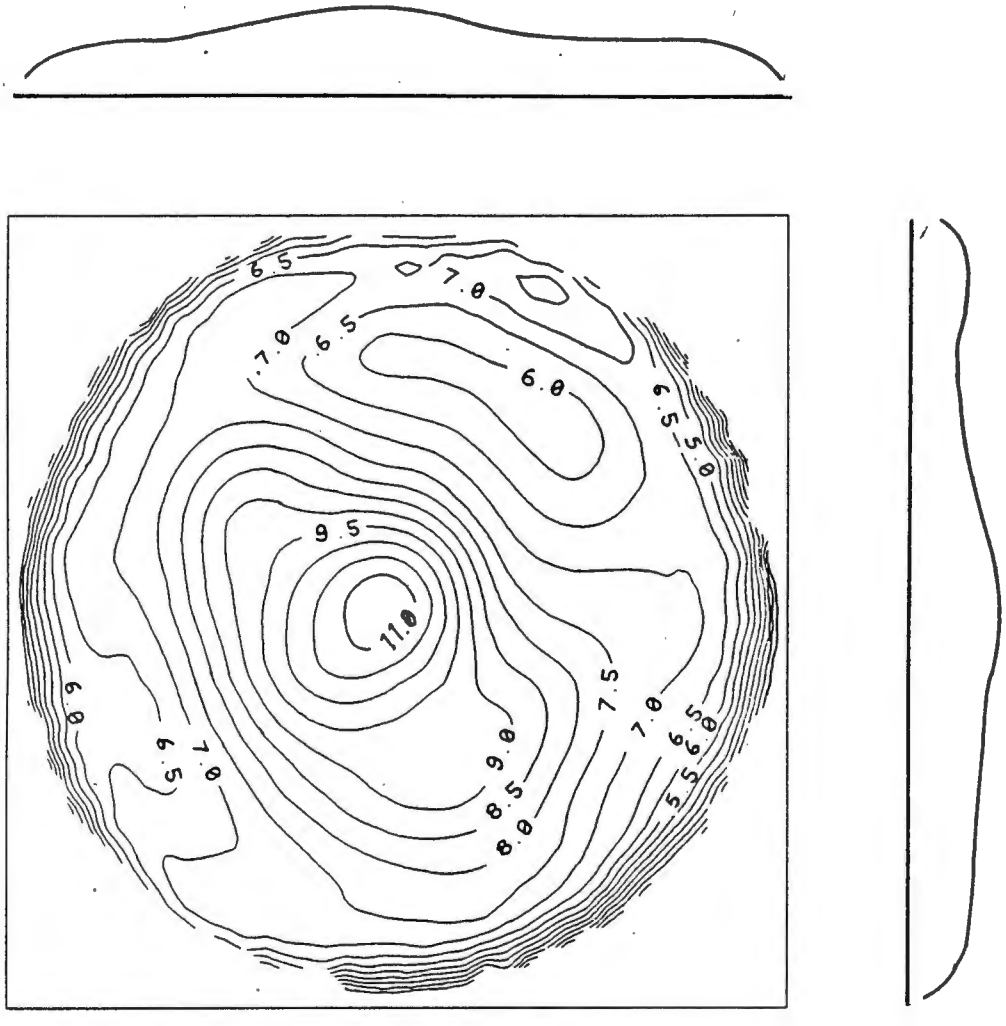

Test No 061004 (Complete tearing, 100%)

Impulse - 49,64 N.s
Mid-point Deflection - 8,0 mm (3mm is taken as the zero on the contour plot)

FIGURE 2.11f CONTOUR PLOT AND DEFORMATION PROFILES OF A DEFORMED PLATE

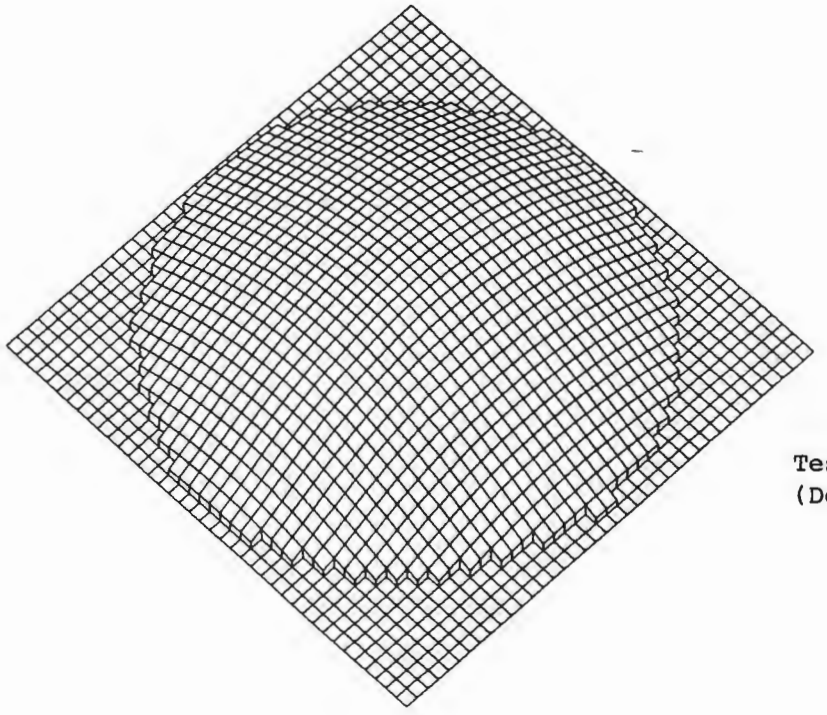

Test No 041006
(Deformation Only)

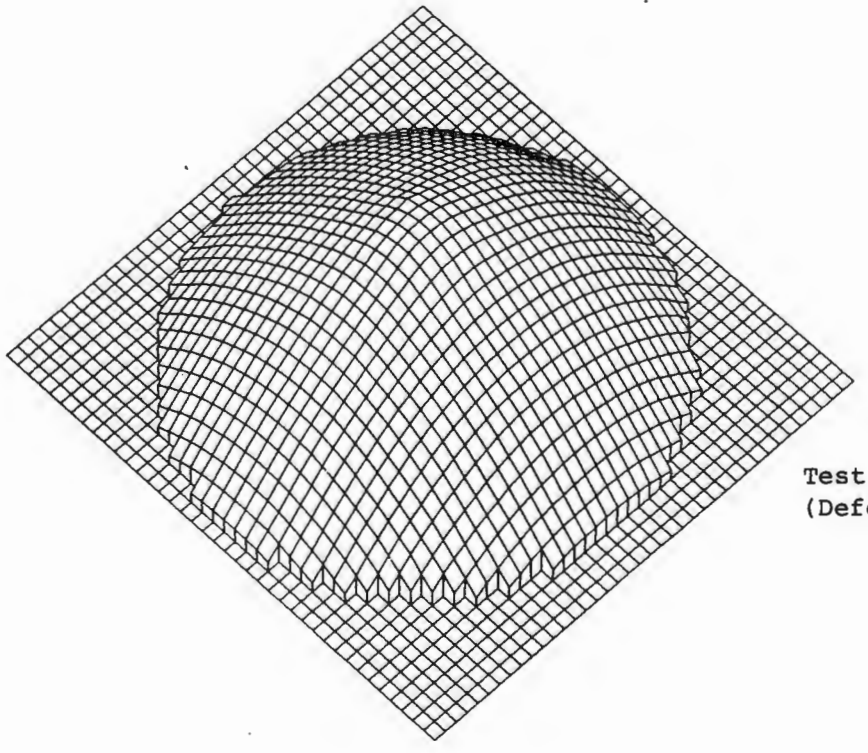

Test No 041007
(Deformation Only)

FIGURE 2.12a THREE DIMENSIONAL PLOTS OF DEFORMED PLATES

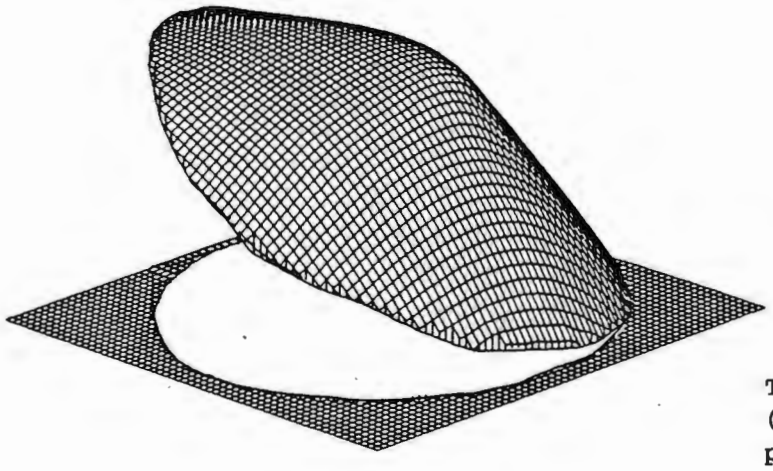

Test No 130402
(Deformation with
partial tearing)

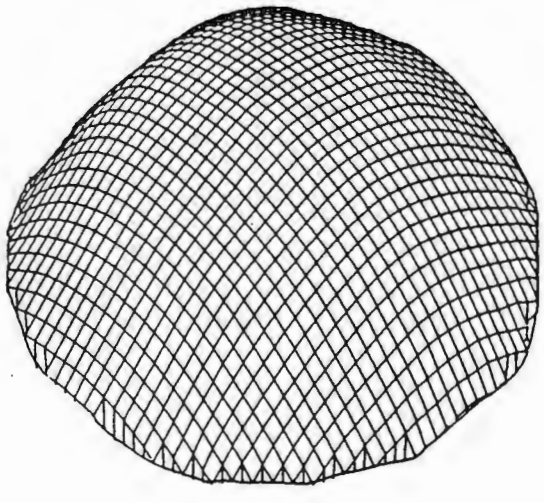

Test No 151001
(Complete tearing)

FIGURE 2.12b THREE DIMENSIONAL PLOTS OF DEFORMED PLATES

Test No 250902
(Complete tearing)

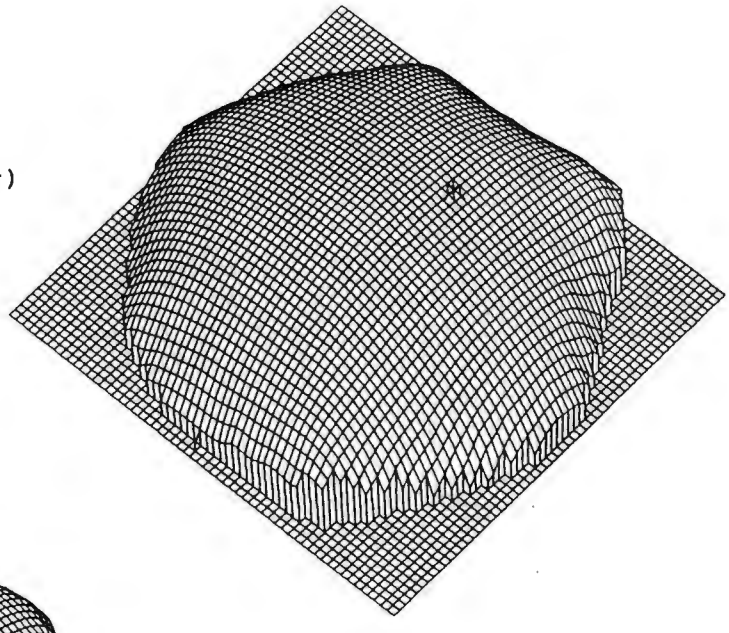

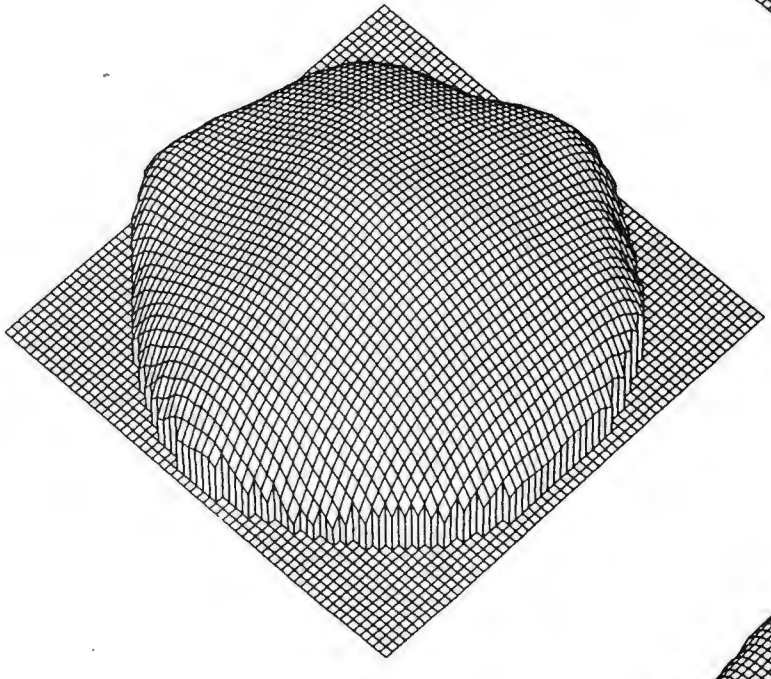

Test No 061001
(Complete tearing)
See photograph Fig 2.2

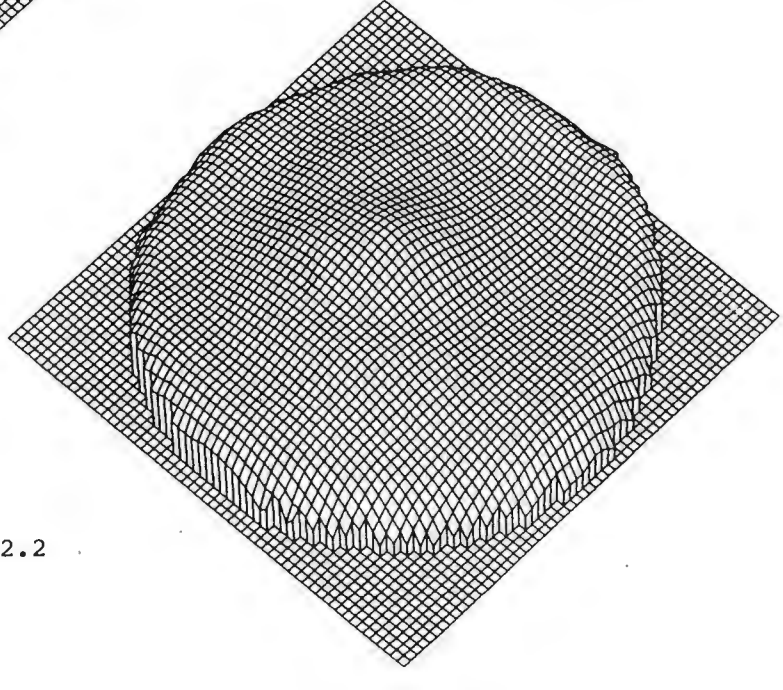

Test No 061004
(Complete tearing)
See photograph Fig 2.2

FIGURE 2.12c THREE DIMENSIONAL PLOTS OF DEFORMED PLATES

TABLE 2.3 TEST DATA

Test No	Explosive Mass (g)	Impulse (N.s)	Measaured Mid-Point Deflect-ion (mm)	Deflection-Thickness Ratio	Velocity of Disc ($m.s^{-1}$)
210903	14,0	4,76	3,6	2,3	
041006	5,5	13,28	12,5	7,8	
041005	6,0	16,85	16,5	10,3	
041004	7,0	17,75	18,2	11,4	
041003	7,5	18,65	18,9	11,8	
041002	8,0	17,75	19,0	11,9	
041001	9,0	21,69	22,7	14,2	
041007	10,0	24,56	25,3	15,8	
041008	11,0	29,24	30,1	18,8	
051002	11,5	26,34	27,3	17,1	partial tearing
051005	11,6	26,17	26,2	16,4	partial tearing
051008	11,65	25,63	24,4	15,3	partial tearing
051009	11,65	28,15	25,3	15,8	partial tearing
051010	11,65	28,86	29,7	18,6	partial tearing
051003	11,75	29,77	26,8	16,8	104,3
051004	11,75	30,67	24,1	15,1	172,7
041009	12,00	29,41	30,9	19,3	partial tearing
051001	12,00	30,31	24,1	15,1	170,2
061002	14,00	32,48	disc squashed		242,4
220901	14,00	32,66	25,0	15,6	no reading
101101	14,00	34,29	disc squashed		271,7
250901	15,00	36,65	21,2	13,3	250,0
220902	15,00	40,48	20,6	12,9	292,7
270902	16,00	36,65	20,3	12,7	210,5
270901	16,00	37,37	19,2	12,0	230,8
250902	16,00	35,57	20,6	12,9	247,4
061001	16,00	39,56	16,3	10,2	300,0
101102	17,00	37,75	16,3	10,2	324,7
250903	17,00	41,37	20,0	12,5	266,7
250904	18,00	39,38	15,9	9,9	285,7
250905	19,00	42,12	14,8	9,3	no reading
250906	20,00	42,66	15,4	9,6	315,8
101103	20,00	43,58	11,7	7,3	362,3
061004	20,60	49,64	8,0	5,0	342,9
250907	21,00	49,46	10,2	6,5	375,0
270903	22,00	47,25	12,6	7,9	393,4
101104	23,00	46,88	10,9	6,8	no reading
061005	23,00	48,53	8,9	5,6	375,0
101105	26,00	52,05	5,0	3,1	423,7

2.6 EXPERIMENTAL OBSERVATIONS

During mode II failure it is observed that as the impulse increases a certain amount of wrinkling occurrs around the circumference of the metal disc, clearly seen in Figure 2.13a. It was noticed in all cases that six ears are present and they are approximately symmetrical. Figure (2.13b) shows a three dimensional plan view of the disc with the six ears clearly visible. Figure 2.13b also shows that the circumference of the disc is not circular. As the threshold impulse for mode III is approached the circumference is observed to become more circular and the presence of the earing is less noticeable. Earing is also found to occur in deep drawing and is defined as the wavy edge on the top of a drawn cup. The earing present in the process of deep drawing is contributed to the directionality in the mechanical properties produced by rolling and other primary working processes. It is mentioned by Dieter [15] that usually two, four or six ears are formed during deep drawing depending on the preferred orientation in the plane of the sheet. It is not however the intention to give an explanation for this phenomena in this thesis but only to note that it is happening and recommend that further work be carried out on the reasons for its occurrence.

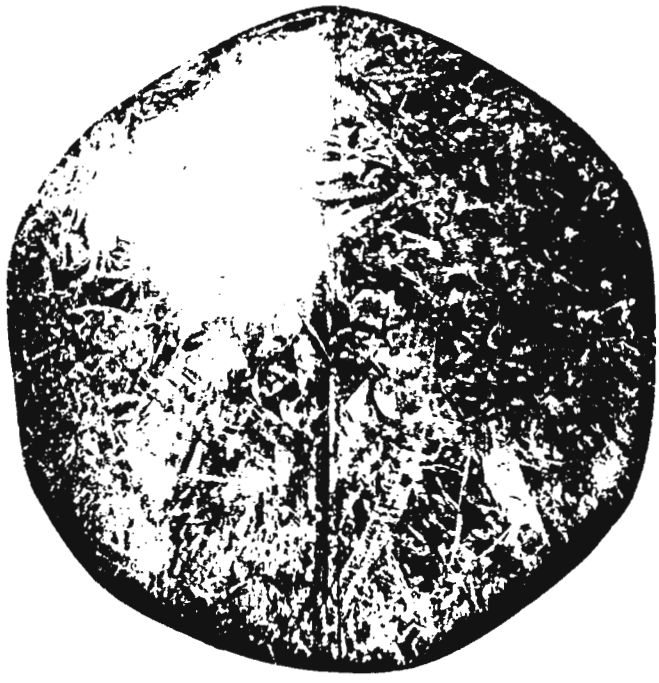

PLAN VIEW

SIDE VIEW

TEST NO : 061001

IMPULSE : 39,56 N.s

FIGURE 2.13a PHOTOGRAPH SHOWING THE WRINKLING OF THE METAL DISC

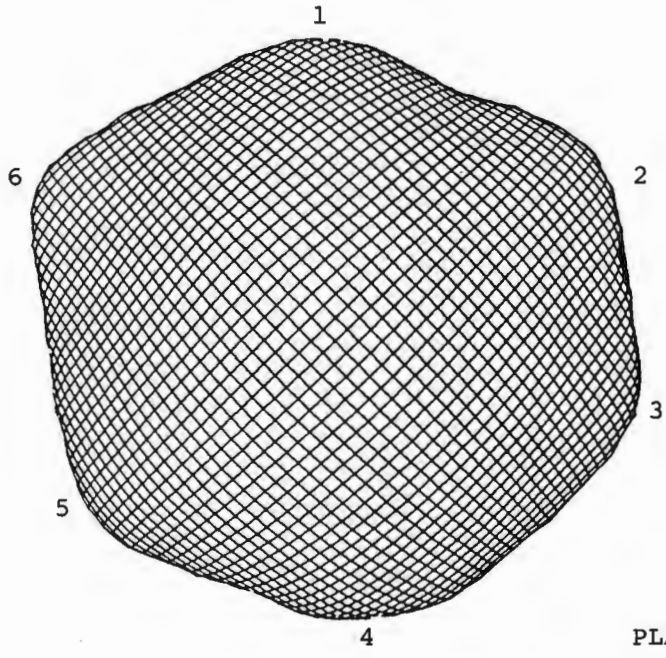

PLAN VIEW

Test No 061001

IMPULSE - 39,56 Ns

FIGURE 2.13b ILLUSTRATION OF THE SYMMETRICAL NATURE OF THE SIX EARS ASSOCIATED WITH THE WRINKLING OF THE METAL DISC

The second observation noted, again one which is not explained, is the nature of deformation of the clamping holes near the plate edge during the different modes of failure. It is noted that during mode I failure the deformation of the holes and associated metal 'stretching' increases as the impulse increases. Maximum stretching is noticed when partial tearing occurrs just before the onset of mode II failure. Once complete tearing has occurred the visible 'stretching' is found to disappear. Figure 2.14 shows this phenomena and the difference in the deformation of the clamping holes during the upper limit of mode I failure and during mode II failure can be seen.

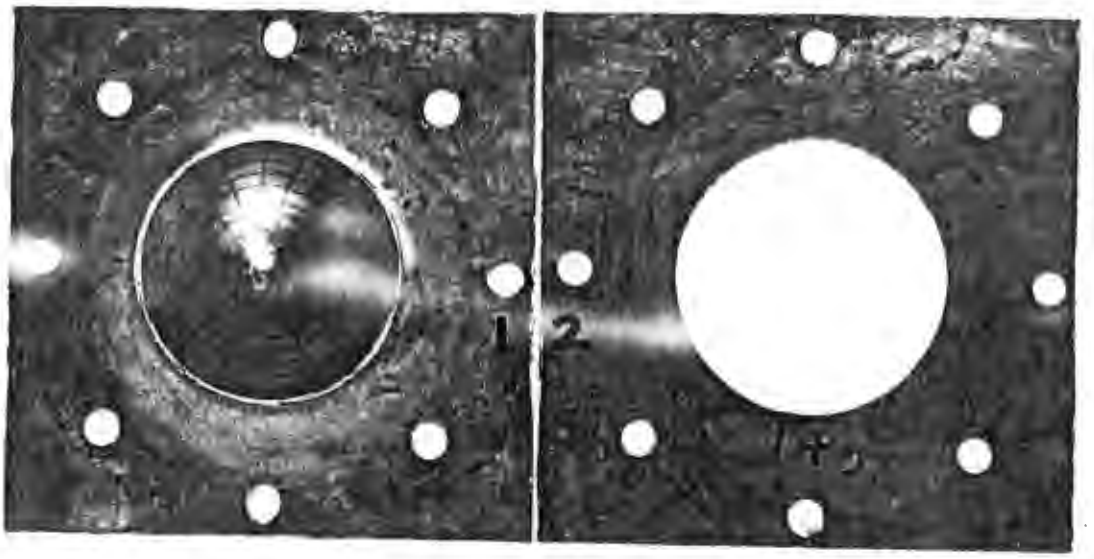

051005

I = 30,31 N.s

220901

I = 32,66 N.s

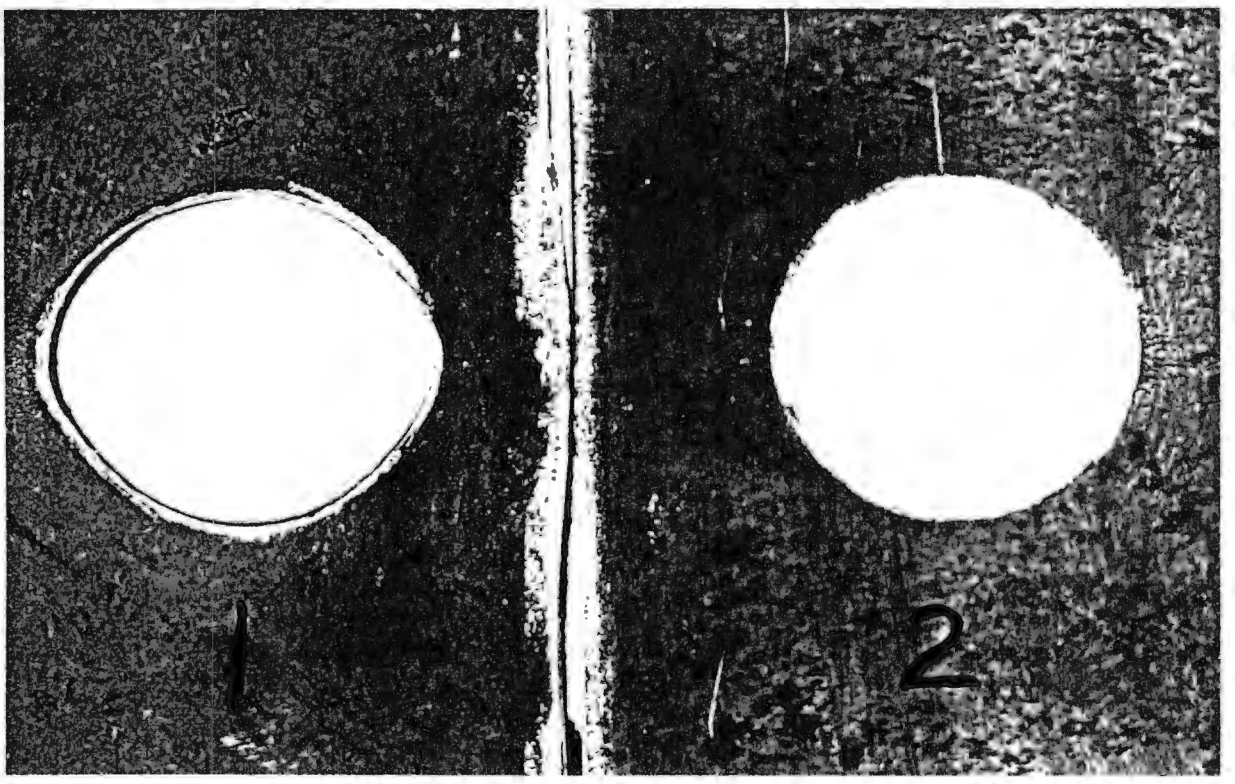

FIGURE 2.14 PHOTOGRAPH COMPARING THE DEFORMATION OF THE CLAMPING HOLES

CHAPTER 3 - THEORETICAL INVESTIGATION

3.1 INTRODUCTION

No work has been found on the tearing of circular plates subjected to an impulsive load. However work has been done on the study of the dynamic response of clamped and simply supported beams subject to very high transverse pressures of extremely short duration. Menkes and Opat [2] conducted a set of experiments in 1973 and observed that as the load on clamped beams is increased, three damage modes are identified. In an attempt to develop a suitable theory to correlate with the experiments Menkes and Opat found that the lumped parameter, finite-difference numerical methods described by Witmer in 1963 are reasonable for the range of inelastic deformation but fall short in that they cannot provide a detailed presentation of stress or strain distribution through the beam thickness near the points of support. If a transverse shear failure occurs, it will take place long before there is any opportunity for significant plastic deformation to occur. Menkes et al [2] therefore suggested that it may be possible to develop a correlation between an experimentally observed shear threshold and a shear-stress resultant obtained by a pseudoelastic analysis. By using Timoshenko beam theory, the shear threshold appears to be dependent on the section velocity,

rather than upon the shear stress. Karunes et al [16] in 1960 suggested the probable incidence of shear failure at very high initial velocities.

Jones [9] in 1976 examined the plastic failure of ductile beams loaded dynamically and uses rigid-plastic methods to predict the large inelastic deformations of the fully clamped impulsively loaded beams, and to estimate the threshold velocities at which failure due to tensile tearing occurs. Jones [17] in 1989 showed how the rigid-plastic methods of analysis could be modified to predict the dynamic failure of beams. His theoretical predictions are however developed for beams made from a strain-rate-insensitive material while in this investigation strain-rate-sensitive material is used. A correction factor to take into account the work hardening of the material is therefore needed before comparison between threshold velocities is made. Jones [9] however found that the threshold velocity for the onset of transverse shear failure is dependent on only the yield stress and density of the test material. When making comparisons the correction factor is applied to the yield stress.

Symonds and Wierzbicki [18] (1978) during their work on the impulsive loading of fully clamped circular plates of perfectly plastic or rate sensitive behaviour use a mode approximation technique, on large

deflections of a symmetrically loaded circular plate, with consideration of strain rate dependence in the plastic behaviour. It is this consideration of the variation of the dynamic yield stress with increasing strain rates that enables previous work done on strain rate insensitive materials and strain rate sensitive materials with small deflections to be used in this investigation.

With the two different processes involved in the failure of the impulsively loaded circular plates, namely deformation and tearing it seems appropriate to develop energy solutions which enable analysis procedures for predicting deformations in structural elements when transient behaviour is of little interest. By using the analysis of the energy required for a certain deformation in the region of pure deformation this can then be used to determine the energy required for a certain deformation after complete tearing has occurred.

Cole [19] in 1948, by assuming a suitable deformed profile, found the energy of deformation by simply considering the work done in providing the increased surface area of the membrane. This method is further refined by Noble and Oxley [4] in 1964 who introduced a factor which takes into account the work-hardening of a particular material. The estimate without the

work-hardening correction gives very poor correlation with the required energy and although the work-hardening factor improves the estimate it is still below that found during experimentation. Lippmann [20] in 1974 deals with the energy approximation in a more complicated manner, by starting from Tresca's yield condition and the associated flow, it is possible to reduce the problem to one single-order partial differential equation which can be solved numerically in a straightforward manner. Lippmann uses this to derive an approximate analytical solution by assuming that the material of the membrane moves vertically downwards only.

The dynamic rigid-plastic energy solutions began in the 1950's when Lee and Symonds [21] used the static plastic-hinge concept, considered beam inertia, and propagated a travelling hinge to analytically obtain the upper bound for permanent deformation in a beam under transverse load. Westine and Baker [22] (1974) then reported that SR Bodner, W Prager, N Jones, JB Martin, RM Haythornthwaite and others then added refinements. Westine and Baker go on to report that JE Greenspan in the 1960's pointed out that one could obtain solutions without going through the details of propagating a plastic hinge along structural members. Greenspan noted that the residual strain energy stored in a plastically deformed member could be calculated

by assuming a final deformed shape. This strain energy was then equated to the energy flux in an explosive blast wave. Westine and Baker [22] disagree with this last step, which made deformations independent of structural orientation relative to the enveloping blast wave, thus ignoring an important effect observed in many experiments. In addition, Greenspan's procedure makes pressures and impulses in the blast wave obey the relationship PI = constant, whose asymptotes for both pressure and impulse are P = O and I = O. Westine and Baker however mention that the response of real targets is related to non-zero P and I limits, so this conclusion was found by them to be unacceptable.

When durations are long relative to the structural response time, the strain energy is equated to the work performed when the peak load moves through the distance that the structure deforms. Hence Westine and Baker noted that two separate procedures are required, one to obtain the solution for the impulsive loading realm, and the other to obtain the solution for the quasi-static loading realm. They showed that:

1) To estimate the impulsive loading realm structural deformation asymptote, estimate the strain energy

2) To obtain the quasi-static structural deformation asymptote, equate the strain energy to the work performed by the peak force deflecting with the structure.

Duffey [1] uses a simplified energy method for rigid plastic material behaviour and equates the strain energy to the initial kinetic energy imparted to the circular plate. Several deformed shape profiles are assumed, including sinusoidal and various polynomial forms to find the best fit to the experimental results.

3.2 ENERGY ANALYSIS

3.2.1 Introduction

Duffey's energy method provides the best correlation with the experimental results (see Table 4.1) and therefore the energy analysis used is based on the rigid-plastic analysis adopted by Duffey [1] and predicts the energy required for the final deformation of a clamped circular plate. The analysis is relatively sensitive to the deflection shape assumed. The shape approximation function as well as the influence of the strain-rate sensitivity and strain hardening of the mild steel will be looked at in sections 3.3 and 3.4.

3.2.2 Rigid Plastic Analysis

The detailed analysis is presented in Appendix B with the plastic strain energy being calculated by

$$E_p = \pi t \int_0^R \sigma_{rr} \left(\frac{\partial \omega}{\partial r}\right)^2 r dr \qquad (3.1)$$

The radial yield stress is

$$\sigma_{rr} = \frac{\sigma_y}{(1 - \nu + \nu^2)^{\frac{1}{2}}} \qquad (3.2)$$

By assuming a deflection shape of the form

$$\omega = \omega_o \phi(r) \text{ where } \phi(r) \text{ is the shape function}$$

the energy required for the deformation of a plate can be calculated from equation (3.1) and a modified version of equation (3.2) using the dynamic yield stress σ_o^1 as calculated in section 3.3.

A simple energy balance can be set up. For mode I failure, with only deformation

$$E_{input} = E_{deformation} \qquad (3.3a)$$

For mode II failure

$$E_{input} = E_{deformation} + E_{tearing} + E_{disc} \qquad (3.3b)$$

For mode III failure where there is no deformation the energy balance would be

$$E_{input} = E_{tearing} + E_{disc} \qquad (3.3c)$$

The input Energy is simply related to the applied impulse and can be calculated as follows

$$E_{input} = \frac{I^2}{2\rho\, t\pi R^2} \qquad (3.4)$$

The energy of deformation is calculated by combining equations (3.1) and (3.2) and using the dynamic yield stress in equation (3.2) we obtain

$$E_{deformation} = \pi t \int_0^R \frac{{\sigma_o}^1}{(1 - \nu + \nu^2)^{\frac{1}{2}}} \left(\frac{\partial \omega}{\partial r}\right)^2 \, r\,dr \qquad (3.5)$$

During mode I failure the values of equation (3.4) and (3.5) should be comparable.

When mode II and mode III failures appear two extra terms come into effect in the energy balance equation, one term to describe the excess energy in the system ie. the energy of the circular deformed disc after

complete tearing has taken place, the other term is the energy required for the tearing of the disc.

The energy of the disc is simple to measure from the velocity as

$$E_{disc} = \tfrac{1}{2}mV_{disc}^2 \qquad (3.6)$$

By combining equations (3.4), (3.5) and (3.6) equation (3.3b) becomes

$$\frac{I^2}{2\rho t\pi R^2} = \pi t \int_0^R \frac{\sigma_o l}{(1-\nu+\nu^2)} \left(\frac{\partial\omega}{\partial r}\right)^2 r\,dr + \tfrac{1}{2}mV_{disc}^2 + E_{tearing} \qquad (3.7)$$

From this it is possible to determine the energy required for tearing of the plate.

3.3 INFLUENCE OF MATERIAL STRAIN-RATE SENSITIVITY AND STRAIN HARDENING

The mode approximation technique presented initially for small deflections of rigid perfectly plastic structures by Martin and Symonds [23] is used by Symonds and Wierzbicki [18] for large deflections of a symmetrically loaded circular plate, with consideration of strain rate dependence in the plastic behaviour. It is this consideration that enables the use of the dynamic yield stress value in calculations for the

different strain rates in the various experimental tests.

In previous similar analyses of impulsive loading, the appropriate dynamic yield stress $\sigma_o{}^1$ was obtained by estimating either empirically or analytically the maximum strain rates during an initial phase of response. In the treatment by Symonds and Wierzbicki [18] the early response involving elastic-plastic bending is omitted.

For the strain rate dependent structural mild steel the relation between the plastic strain rate $\dot{\varepsilon}$ and axial stress $\sigma_o{}^1$ is

$$\sigma_o{}^1 = \sigma_o \left[1 + \left(\frac{\dot{\varepsilon}}{\dot{\varepsilon}_o}\right)^{\frac{1}{n}} \right] \tag{3.8}$$

and can be written as

$$\dot{\varepsilon} = \dot{\varepsilon}_o \left[\frac{\sigma_o{}^1}{\sigma_o} - 1 \right]^n \tag{3.9}$$

Symonds and Wierzbicki [18] found the average strain rate over the response time for circular plates loaded over their entire surface to be

$$\dot{\varepsilon}_r^{AV} = \frac{I^2(0,05365)}{R^5 t^2 \sqrt{\rho^3 \sigma_o{}^1}} \qquad (3.10)$$

Equating equations (3.9) and (3.10), and using the following material properties

$\dot{\varepsilon} = 40\ s^{-1}$

$n = 5$

$\rho = 7850\ kg\ m^{-3}$

$R = 50\ mm$

$t = 1,6\ mm$

produces

$$\frac{I^2\ 96421,8}{\sqrt{\sigma_o{}^1}} = 40\left(\frac{\sigma_o{}^1}{\sigma_o} - 1\right)^5 \qquad (3.11)$$

where I is the applied impulse, σ_o is the uniaxial yield stress and $\sigma_o{}^1$ the required dynamic yield stress.

An iterative calculation is used to solve equation (3.11) for each chosen impulse and σ_o, starting with an approximated value of $\sigma_o{}^1$. Appendix C gives the values of the dynamic yield stress for all the experimental tests.

3.4 SHAPE APPROXIMATION FUNCTIONS

By predicting the deformed shape of the circular plate it is possible to determine the energy required from equation (3.5). Nurick [13] developed a mode approximation technique by the use of membrane analysis to predict the mode shape at five evenly spaced mode points. By using these mode shapes and Stirling's Formula [24] (Appendix D) it is possible to fit a polynomial to a set of data points and thereby develop a shape function. This function is expected to correlate closely to current experimental work due to the close correlation between the experimental work conducted by Nurick and the experimental work performed in this investigation.

Table 3.1 gives the shape function predicted here by using Stirling's Formulae as well as the shape functions used by Westine et al [22], Wang [25] and Duffey [1].

A comparison between the predicted deformation shapes given and the experimentally determined shapes will be given in Chapter 4 where the simplest best fit shape function will be selected for use in the energy solution described earlier in Section 3.2.

TABLE 3.1 **PREDICTED SHAPE FUNCTIONS**

	Shape Function $\phi(r)$	Comments
Polynomial from Stirling's formula, using Nurick's [13] mode shapes (appendix D)	$\omega = \omega_o [0,770 - 0,20467\Theta - 0,3584\Theta^2 + 0,00517\Theta^3 + 0,00033\Theta^4]$	clamped circular plates
Westine and Baker [22]	$\omega = \frac{\omega_o}{2}\left(1 + \cos\frac{\pi r}{R}\right)$	clamped circular plates
Wang [25]	$\omega = \frac{\omega_o}{3}\left(3 - \frac{r}{R} - \left(\frac{r}{R}\right)^2 - \left(\frac{r}{R}\right)^3\right)$	simply supported circular plates
Duffey [1]	$\omega = \omega_o \cos\frac{\pi r}{2R}$	clamped circular plates
	$\omega = \omega_o \left[1 - \left(\frac{r}{R}\right)\right]$	
	$\omega = \omega_o \left[1 - \left(\frac{r}{R}\right)^2\right]$	
	$\omega = \omega_o \left[1 - \left(\frac{r}{R}\right)^3\right]$	

CHAPTER 4 - RESULTS

During testing two different sheets of mild steel are used. Tensile tests are performed on each sheet and the uniaxial yield stress is found to differ by 12,74 MPa. A dimensionless number is used to compare the individual results and compare results with previous work and is given by,

$$\phi = \frac{I\ (1 + \ln \frac{R}{R_o})}{\pi R t^2 (\rho \sigma_o)^{\frac{1}{2}}} \qquad (4.1)$$

where R_o is the radius of plate over which the impulse is imparted. For the case of uniform loading presented here R_o = R and therefore equation 4.1 reduces to

$$\phi = \frac{I}{\pi R t^2 (\rho \sigma_o)^{\frac{1}{2}}} \qquad (4.2)$$

The ϕ value obtained in the current investigation of 47.2 before visible tearing occurred is greater than the value of 26.07 found by Nurick [6]. This is probably due to the fact that different sheets of mild steel were used in the tests and also material defects could have an effect on the point of initiation of tearing. Although the tearing was clearly visible by Nurick, after closer study of the present test plates it

was found that a small amount of tearing could be seen under a microscope at an impulse of 23 N.s.

A least squares correlation is performed on the data for both mode I failure and mode II failure (Figure 4.1). Mode III failure occurs with complete shearing without any deformation of the disc. The least squares line is bounded by $\pm$ 1 deflection-thickness ratio in each case. For the mode I failure it can be seen that all the data points lie inside these bounds but for the region of mode II failure the scatter is greater with a certain number of points falling outside this bound. The greater degree of inaccuracy in this region is due to the possibility that the circular discs are deformed slightly when caught and also the irregular shapes of some of them (see Figures 2.12 and the photograph in Figure 2.13a) make it difficult to measure the mid-point deflection accurately.

The least squares analysis yields from the plate experimental data for mode I failure

$$\left(\frac{\delta}{t}\right) = 0{,}407\phi - 0{,}957 \quad \text{with} \quad r = 0{,}997$$

and for mode II failure

$$\left(\frac{\delta}{t}\right) = -0{,}318\phi + 32{,}46 \quad \text{with} \quad r = -0{,}937$$

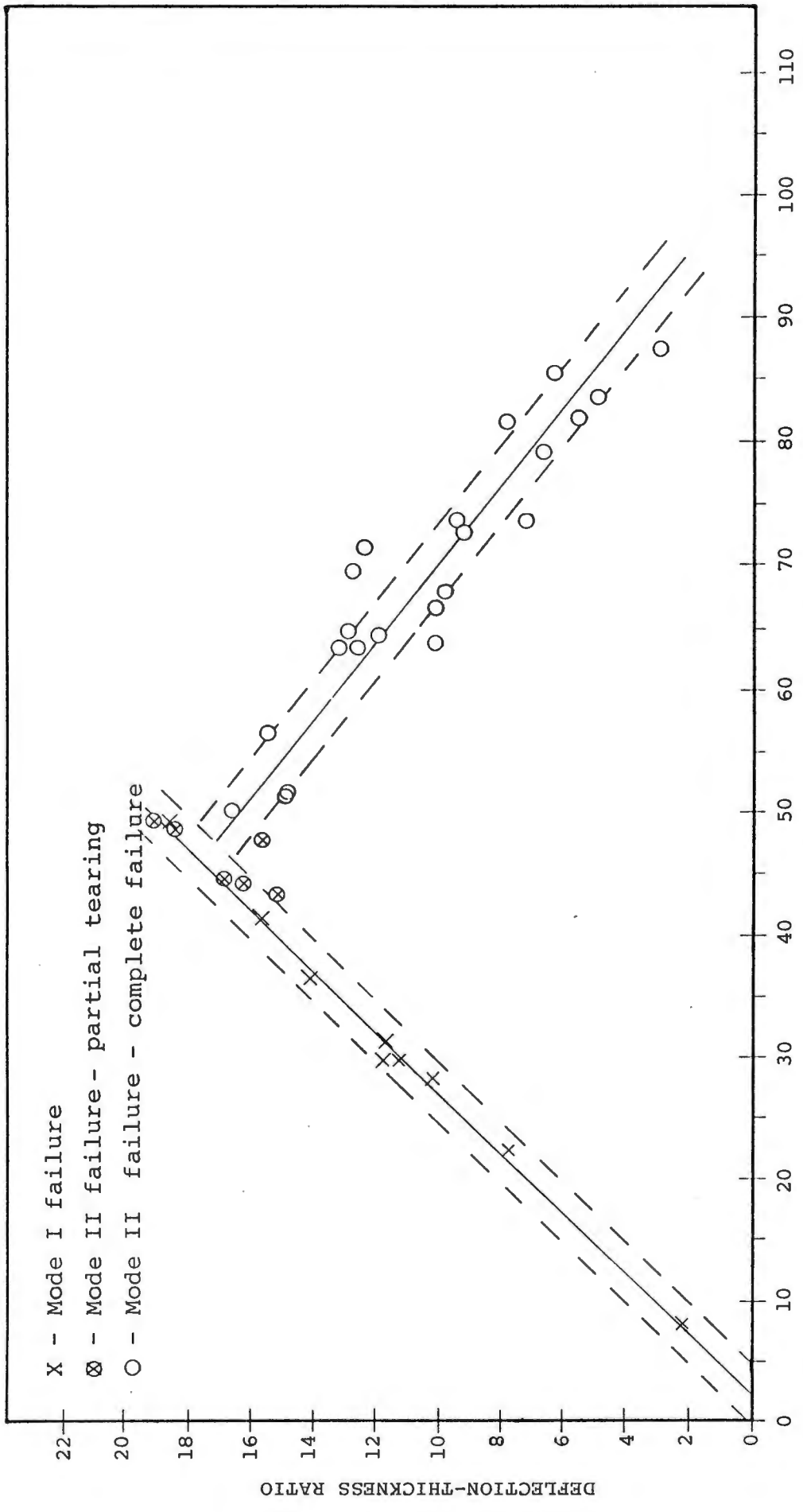

FIGURE 4.1 GRAPH OF DEFLECTION-THICKNESS RATIO vs DIMENSIONLESS NO ϕ WITH A LEAST SQUARES CORRELATION AND $\pm$ 1 DEFLECTION-THICKNESS RATIO

The least squares analysis performed by Nurick [6] for mode I failure gives

$$(\frac{\delta}{t}) = 0,425\phi + 0,277$$

The correlation between these two lines is very good and shows good repeatability of experiments in the mode I failure range, with the experiments in this investigation being performed on the same ballistic pendulum used by Nurick [6].

The predicted shape functions given in Table 3.1 are shown in Figures 4.2a and 4.2b where a comparison is shown for two different test plates. For both shape functions it can be seen that the shape function used by Duffey [1] of

$$w = w_o \cos (\frac{\pi r}{2R}) \qquad (4.3)$$

corresponds very well with the experimental shape. This shape function because of its simplicity is therefore used in equation (3.5) when the energy of deformation is calculated.

Substituting equation (4.3) into equation (3.5) gives

$$E_{deformation} = \frac{\pi^3 t \sigma_o {}^1\omega_o{}^2}{4(1-\nu+\nu^2)^{\frac{1}{2}}} (\tfrac{1}{4} + \frac{1}{\pi^2}) \qquad (4.4)$$

where poisson's ratio (ν) is taken as 0,33 in all applications [26]. The determination of the energy for deformation is the main area of concern and unlike the input energy and disc

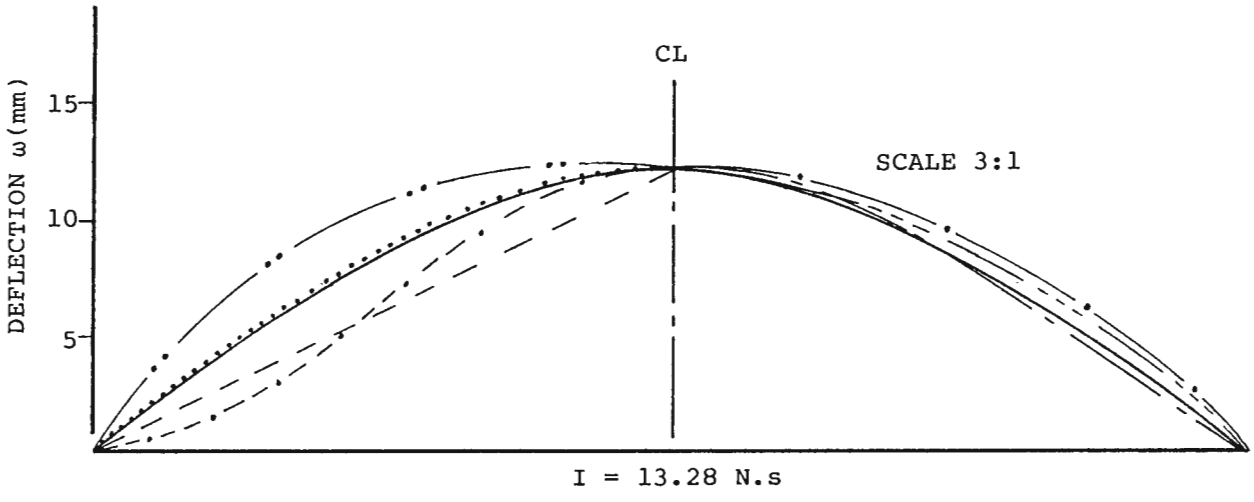

——————— Experimental shape Test no 041006
——— - ——— - ——— Stirling's Forumula (Right of CL) (Nurick (13))
— — . — — . — — . Westine and Baker (Left of CL)
——— --- ——— --- Wang (Right of CL)
— — — — — — — — — Duffey - $\omega_o(1 - \frac{r}{R})$ (Left of CL)
. . . . . Duffey - $\omega_o \cos(\pi r/2R)$ (Left of CL)
—— · —— · ——· Duffey - $\omega_o (1 - (r/R)^2)$ (Right of CL)
—— ·· —— ·· —— Duffey - $\omega_o (1 - (r/R)^3)$ (Left of CL)

FIGURE 4.2(a) COMPARISON BETWEEN EXPERIMENTAL AND PREDICTED SHAPE FUNCTIONS - TEST NO 041006

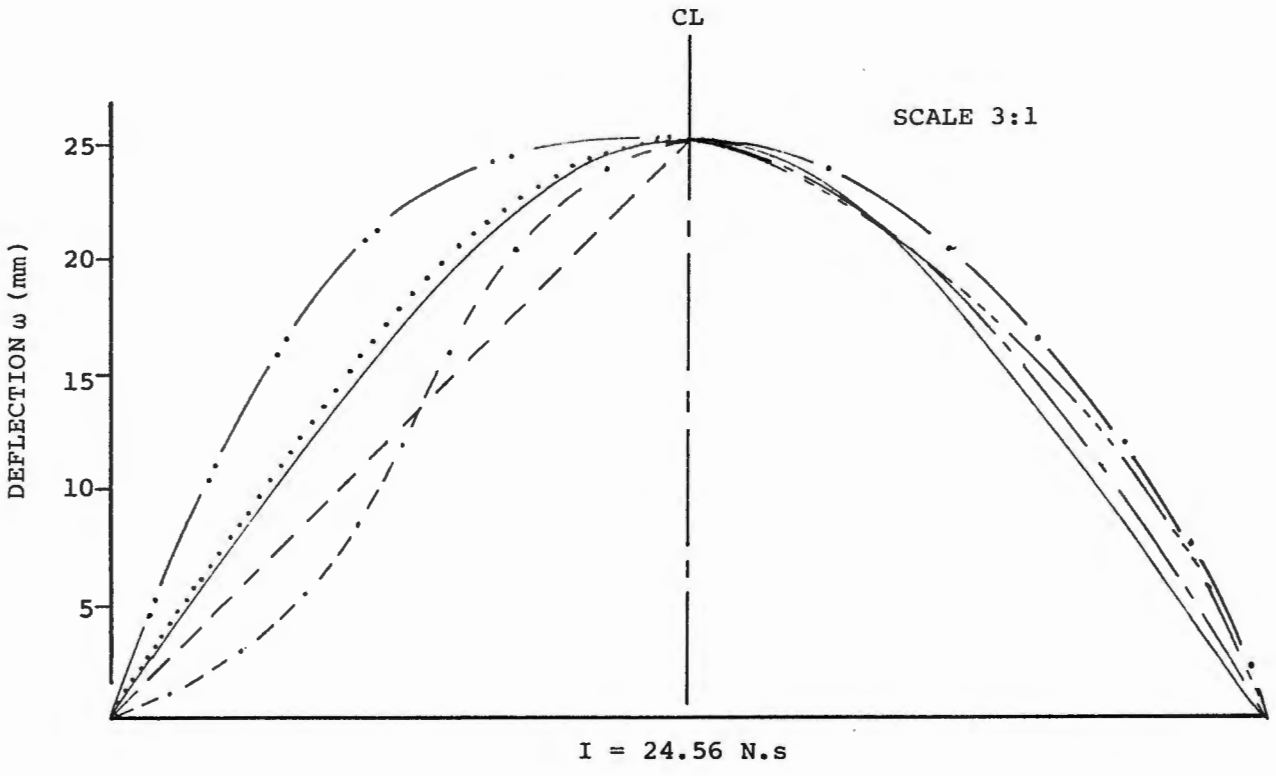

FIGURE 4.2(b) COMPARISON BETWEEN EXPERIMENTAL AND PREDICTED SHAPE FUNCTIONS - TEST NO 041007

energy, the energy of deformation is difficult to predict accurately. Table 4.1 compares the energy of deformation for a mode I type failure with the input energy for two tests. The energy methods of Duffey [1], Westine and Baker [22], Lippman [20] and Noble and Oxley [4] are all shown.

During initial investigation it is expected that the energy of deformation and the input should be equal. However, the values of the energy of deformation predicted by the energy method of Duffey and using the dynamic yield stress show two quite contrasting results. From Table 4.1 it is observed that for the smaller deformation the energy of deformation value is only 70% of the input energy whereas for the larger deformation the value predicted is approximately 97% of the input energy. Before analysing these two values it should be noted that the consideration of complete edge fixity, as assumed in the theories, was difficult to impose in the tests where the plate was clamped by bolts. At the large impulse loads it was found that a small amount of radial slippage occurred. The photograph in Fig 2.14 shows a test plate having been subject to an impulse of 25 N.s and it can clearly be seen from the shape of the holes near the edge (previously circular) that a certain amount of 'slippage' has occurred. The final mid point deflection is sensitive to this condition, and thus for the tests involving large impulses the measured deflections could be slightly larger than they should be (mentioned by Perrone et

TABLE 4.1 COMPARISON BETWEEN DEFORMATION ENERGY AND INPUT ENERGY FOR MODE 1 TYPE FAILURE

Duffey [1] $E_{def} = \frac{\pi^3 t \sigma_y \omega_o^2}{4(1-\nu+\nu^2)^{\frac{1}{2}}}(\frac{1}{4} + \frac{1}{\pi^2})$

Westine and Baker [22] $E_{def} = \frac{\pi^2 \sigma_y t^2 \omega_o}{4} + \frac{1}{16}(\pi^3 \sigma_y t \omega_o^2)$

Lippman [20] $E_{def} = 0,423 \rho t R^2 \ (\omega_o \pi / 1,306\ R(\rho/\sigma_y)^{\frac{1}{2}})^2$

Noble and Oxley [4] $E_{def} = t \sigma_y \Delta A$

Test No 041006 $\sigma_o = 277,04$ MPa

$\sigma_o^1 = 749,37$ MPa $\omega_o = 12,5$mm

INPUT ENERGY = 829,15J

	E_{def} Using $\sigma_y=\sigma_o$	% of E_{input}	E_{def} Using $\sigma_y=\sigma_o^1$	% of E_{input}
Duffey	213,72	25,8	578,08	69,7
Westine & Baker	156,09	18,8	422,22	50,9
Lippman	169,53	20,4	458,55	55,3
Noble & Oxley	200,53	24,2	542,4	65,4

Test No 041007 $\sigma_o = 277,04$ MPa

$\sigma_o^1 = 871,95$ MPa $\omega_o = 25,3$mm

INPUT ENERGY = 2835,00J

	E_{def} Using $\sigma_y=\sigma_o$	% of E_{input}	E_{def} Using $\sigma_y=\sigma_o^1$	% of E_{input}
Duffey	875,50	30,9	2 755,53	97,2
Westine & Baker	594,11	20,9	1 869,89	66,0
Lippman	694,48	24,5	2 185,78	77,1
Noble & Oxley	603,99	21,3	1 900,99	67,1

al [29] in connection with the experiments conducted by Bodner and Symonds). This means that the mid-point deflection used to calculate the values of the energy of deformation could be inflated and therefore the predicted percentage could be lower than 97,2%. This does not however, explain why there is a discrepancy between the input energy and the predicted deformation energy.

The impulse measurement calculated from the deflection of the pendulum is used in the calculation of the total input energy imposed on the plate. This means that a very important assumption has been made, namely that the high intensity gas pressures from the explosion act only on the specimen surface; thus the pendulum itself is assumed to have no external forces other than those exerted by the specimen through its support reactions. There is however, the possibility that unwanted impulsive pressures might have imparted additional momentum to the pendulum block, so resulting in a slightly inflated impulse measurement (mentioned previously by Symonds et al [30]). This could in some way explain the discrepancies between the energy of deformation and input energy in mode I failure.

Once the input energy, deformation energy and energy of the disc have been determined the energy of tearing can be found from equation (4.5).

$$E_{tearing} = E_{input} - (E_{deformation} + E_{disc}) \qquad (4.5)$$

Figure 4.3 shows a plot of the energy versus the dimensionless number ϕ. Least squares correlation [28] has been performed on the relevant sets of data, and equations for these curves with the boundary conditions for ϕ are given below:

$$E_{input} = 1,822\phi^{1,991} \quad \phi \geq 0 \tag{4.6}$$

$$E_{disc} = 175,96\phi - 7962,0 \quad \phi \geq 47 \tag{4.7}$$

$$E_{deformation} = \frac{32\ 4835,34}{\phi} - 3350 \quad 47 \leq \phi \leq 97 \tag{4.8}$$

$$E_{tearing} = 124,22\,\phi - 5896,9 \quad \phi \geq 47 \tag{4.9}$$

The limits of ϕ in the energy equations are only approximate and have been determined purely by observation.

The ϕ value of 47 indicated in the limits indicate the threshold value for the onset of mode II failure. The threshold value for the onset of mode III failure is difficult to determine because of the lack of experimental data in the region involving very high impulsive loads. It is however predicted that this value occurs between the ϕ values of 85 and 95 (Figure 4.4).

The corresponding threshold impulses and initial deformation velocities, assuming σ_o = 277,04 MPa, are:

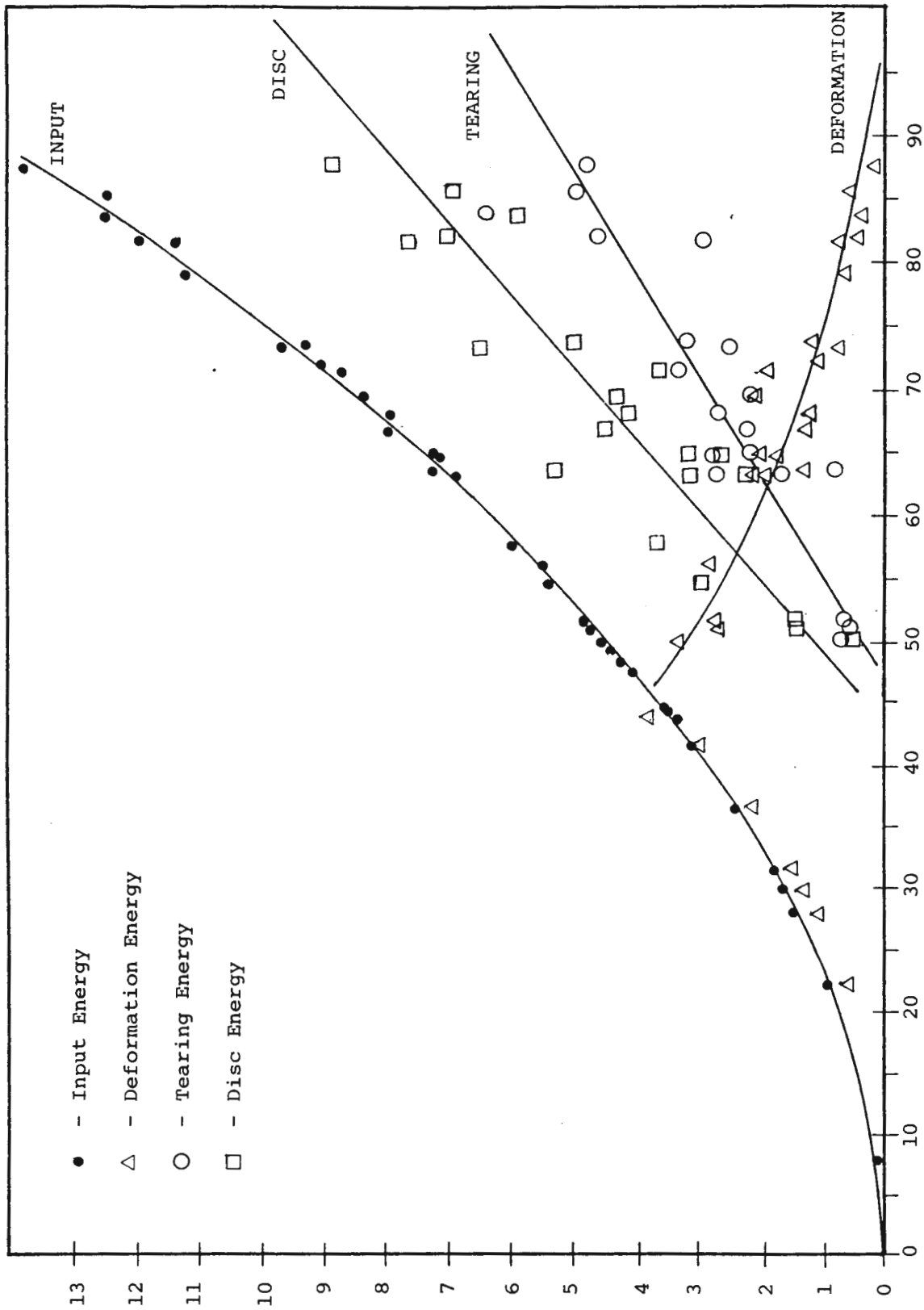

FIGURE 4.3 GRAPH OF ENERGY VERSUS DIMENSIONLESS NO ϕ SHOWING LEAST SQUARES CORRELATION

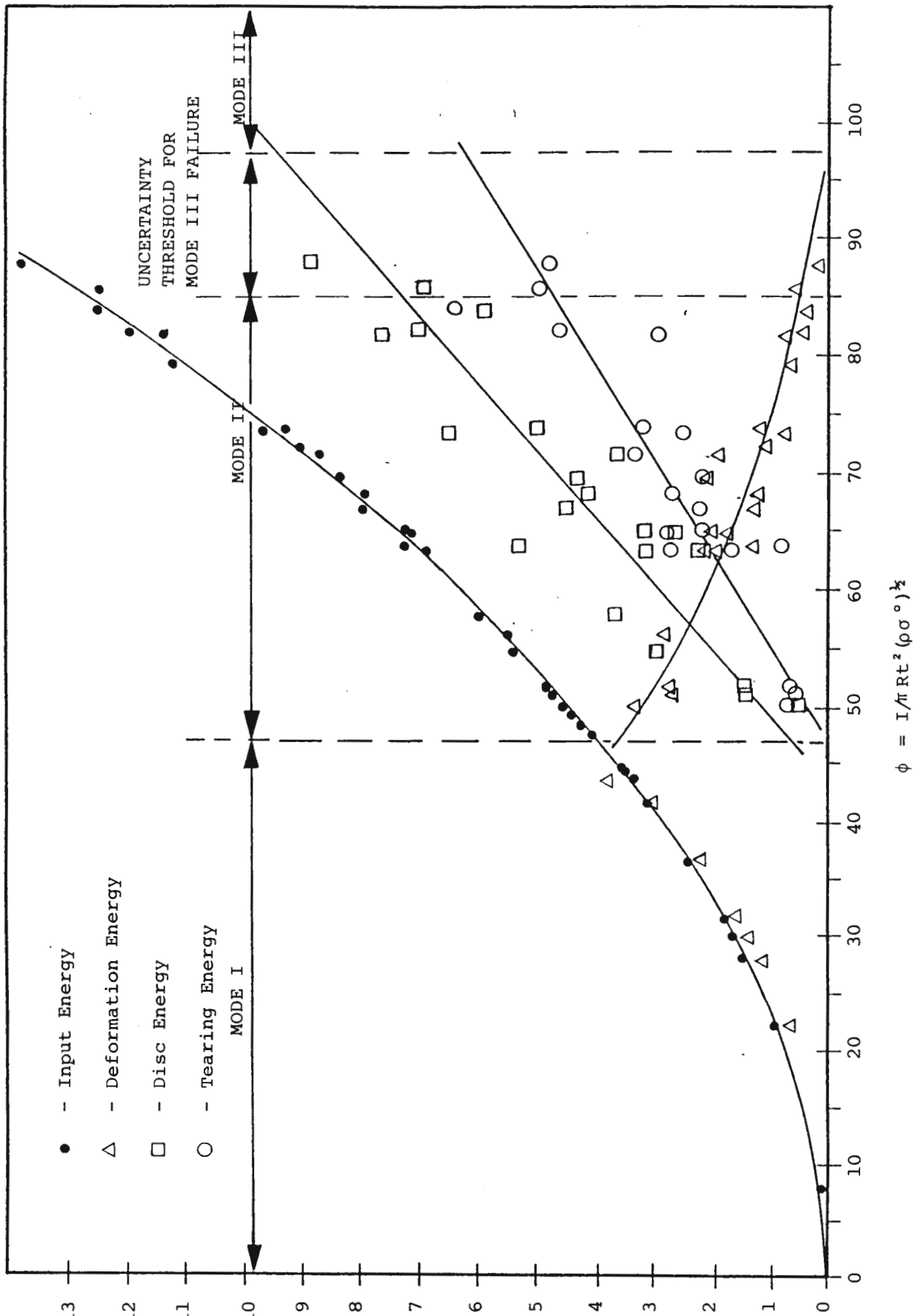

FIGURE 4.4 GRAPH OF ENERGY VERSUS DIMENSIONLESS NO ϕ SHOWING THE 3 MODES OF FAILURE

Using $I = \phi \pi R t^2 (\rho \sigma_o)$

and $V_o = I/\rho\, t\, \pi\, R^2$

$\phi = 47$ $I = 27,9$ N.s $V_o = 282,8$ m.s^{-1}

$\phi = 85$ $I = 50,4$ N.s $V_o = 511,0$ m.s^{-1}

$\phi = 95$ $I = 56,3$N.s $V_o = 570,7$ m.s^{-1}

The threshold velocity predicted by Jones (8) for the onset of mode 3 behaviour in the failure of ductile beams was

$$V_o = \frac{2\sqrt{2}}{3} \left(\frac{\sigma_o}{\rho}\right)^{\frac{1}{2}} \qquad (4.10)$$

In equation (4.10) we replace σo with $\sigma^1 o$ to take into account the strain rate sensitive behaviour of the mild steel

therefore $V_o = \frac{2\sqrt{2}}{3} \left(\frac{\sigma_o{}^1}{\rho}\right)^{\frac{1}{2}}$

For $I = 50,4$ N.s $\sigma o^1 = 1066,2$ MPa

therefore $V_o = 347,5$ m.s^{-1}

This is much lower than the value found in experimentation and therefore for the case of the circular plates the assumption cannot be made that the value of the threshold velocity for mode III failure is independent of the geometry of the test plate.

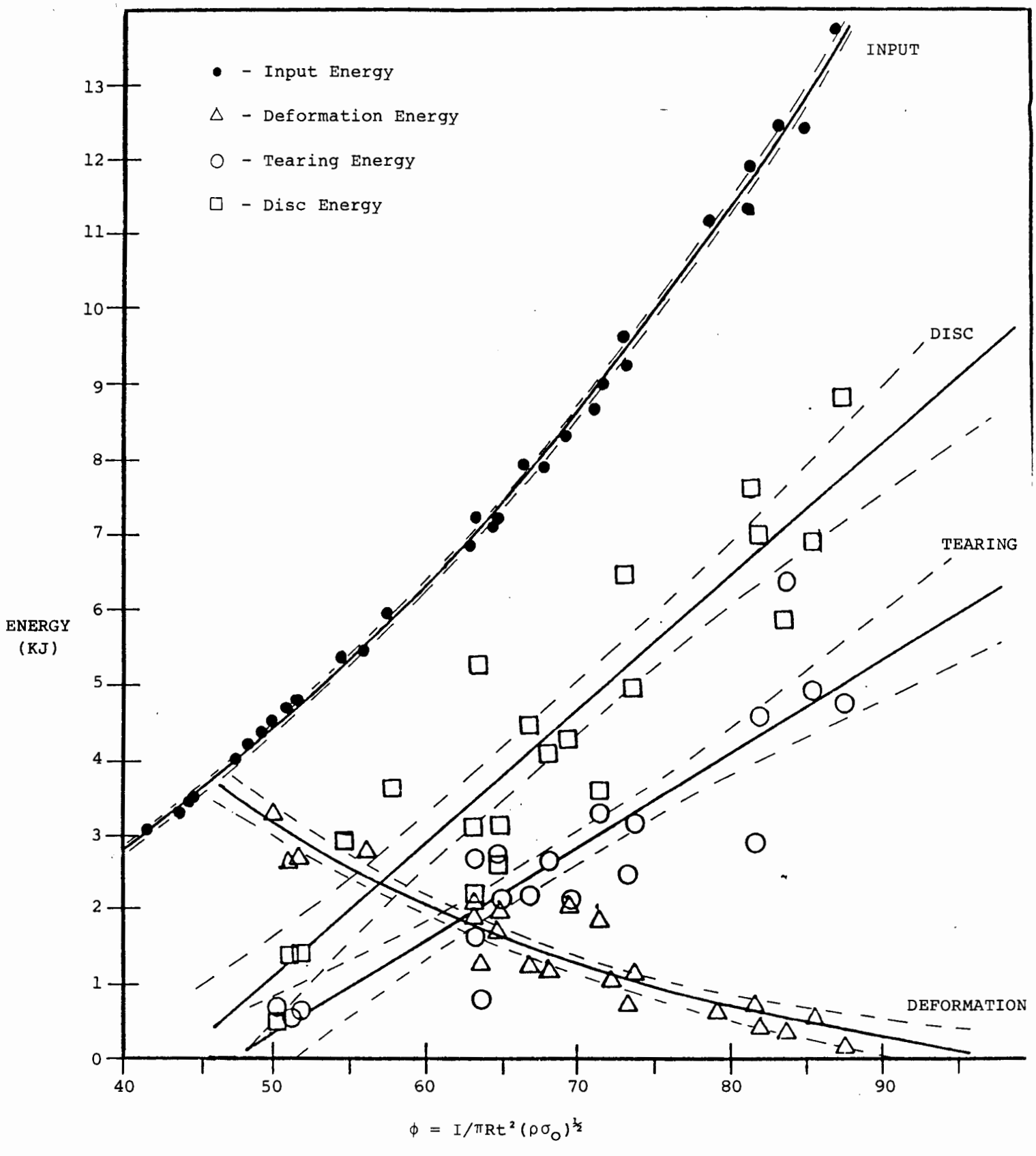

FIGURE 4.5 GRAPH OF THE ENERGY VERSUS DIMENSIONLESS NO ϕ SHOWING A 90% CONFIDENCE RANGE OF CORRELATION

A statistical analysis was performed on the experimental data (Appendix E [27]) and Figure 4.5 shows a plot of the energy versus dimensionless number with a 90% confidence range of correlation.

CHAPTER 5 - DISCUSSION AND CONCLUSIONS

This thesis presents an experimental study on the failure of impulsively loaded circular plates. Three failure modes are identified, inelastic deformation, tearing at the supports and transverse shear at the supports.

The experimental procedure described in Chapter 2 describes how by using a ballistic pendulum and loading a clamped circular plate with an impulse load the impulse imparted on the plate is measured. The loading is produced by the detonation of plastic explosive and it is found that correlation between the mass of explosive used and the impulse measured is not sufficiently good to allow the use of a separate set of calibration tests to calculate a specific impulse giving the impulse per unit mass of explosive. The experimental technique used is shown to be reproducible and consistent providing the velocity of the metal disc (when necessary) while simultaneously measuring the impulse.

Analysis of the experimental data produced equations to determine the deflection-thickness ratio for a certain impulse. These two terms were related using a dimensionless number ϕ.

For mode I failure the least squares line produces

$$\left(\frac{\delta}{t}\right) = 0{,}407\phi - 0{,}957 \quad \text{where} \quad \phi \leq 47$$

The least squares line for mode II failure yields

$$\left(\frac{\delta}{t}\right) = -0,318\ \phi + 32,46 \quad \text{where } 47 \leq \phi \leq 97$$

The equation for mode I failure compares very favourably with that determined by Nurick [6] showing the very good repeatability of the experiments in this range. The equation for mode II failure is less accurate as it is difficult to measure accurate mid-point deflections of the circular discs. No work was found on the failure of circular plates by tearing and therefore no comparisons are made.

An energy balance is developed for the range of experimental testing and the following equations apply to the three different modes of failure.

Mode I

$$E_{input} = E_{deformation}$$

Mode II

$$E_{input} = E_{deformation} + E_{tearing} + E_{disc}$$

Mode III

$$E_{input} = E_{tearing} + E_{disc}$$

By measuring the mid-point deflection of the deformed plate and using a predicted shape function the deformation energy can be found. The disc energy is determined by measuring the velocity of the disc and calculating its kinetic energy. The impulse imparted on the plate is used to measure the input energy.

Figure 4.4 shows a plot of the different energies and also shows the boundaries of the different mode failures. Figure 4.5 gives a graph of energy versus the dimensionless number ϕ with boundaries showing a 90% confidence range of correlation.

The threshold velocities for the onset of failure modes II and III were found to be

Mode II $V_o = 282,8 \text{ m.s}^{-1}$

Mode III $V_o \simeq 511,0 \text{ m.s}^{-1}$

No work was found on these two failure modes on circular plates and therefore comparisons have not been made.

CHAPTER 6 - RECOMMENDATIONS

The experimental observations mentioned in Chapter 2 were beyond the limits of the present study and therefore no explanation was given. It is therefore recommended that future work be done in order to explain the following two phenomena.

1. The presence of wrinkling along the circumference of the metal disc during mode II failure and why when mode III failure begins this wrinkling disappears. Also why the wrinkling showed itself in the form of six symmetrical ears in each case.

2. Radial stretching of the plate during mode I failure with no noticeable, radial stretching occurring during mode II and mode III failure.

REFERENCES

1. DUFFEY TA, 1967, **The large deflection dynamic response of clamped circulator plates subjected to explosive loading,** Sandia Laboratories Research Report, SC-RR-67-532.

2. MENKES SB, OPAT HJ, 1973, **Tearing and shear failures in explosively loaded clamped beams,** Exp Mech, Vol 13, pp.480-486.

3. NURICK GN, 1986, **The measurement of the deformation response of a structure subjected to an explosive load using a light interference technique,** Proceedings of the 1986 SEM Spring Conference on experimental mechanics, pp.105-114.

4. NOBLE CF, OXLEY PLB, 1964, **Estimating the charge size in explosive forming of sheet metal,** The College of Aeronautics, Cranfield.

5. JOHNSON W, 1972, **Impact Strength of Materials,** Edward Arnold.

6. NURICK GN, MARTIN JB, 1989, **Deformation of thin plates subjected to impulsive loading - A review,** Int J Impact Eng, Vol 8, pp.159-186.

7. WIERZBICKI T, FLORENCE AL, 1970, **A theoretical and experimental investigation of impulsively loaded clamped**

circular viscoplastic plates, Int J Solids Struct, Vol 6, pp.553-568.

8. BODNER SR, SYMONDS PS, 1979, **Experiments on dynamic plastic loading of frames,** Int J Solids Struct, Vol 15, pp.1-13.

9. JONES N, 1976, **Plastic failure of ductile beams loaded dynamically,** J Eng for Ind, pp.131-136.

10. DUFFEY TA, 1988, **Dynamic Rupture of shells.** Structural failure (T Wierzbicki and N Jones, Eds)) John Wiley (1988).

11. FLORENCE AL, 1966, **Circular Plate Under a Uniformly distributed impulse,** Int J Solids Structures, Vol 2, pp.37-47.

12. BODNER SR, SYMONDS PS, 1979, **Experiments on Viscoplastic Response of circular plates to impulsive loading,** J Mech Phys Solids, Vol 27, pp.91-113.

13. NURICK GN, 1987, **Large deformations of thin plates subjected to impulsive loading,** Phd, University of Cape Town.

14. JONES N, 1986, **Some comments on the dynamic plastic behaviour of structures,** keynote address, proceedings at the International Symposium on Intense Dynamic Loading

and its Effects, Science Press, Beijing, China, pp.49-71.

15. DIETER GE, 1976, **Mechanical Metallurgy**, McGraw-Hill, pp.697-700.

16. KARUNES B, ONAT ET, 1960, **On the effect of shear on plastic deformation of beams under transverse impact loading**, J of Appl Mech, Vol 27, pp.107-109.

17. JONES N, 1989, **On the dynamic inelastic failure of beams**, structural failure, John Wiley and Son Inc, pp.133-159.

18. SYMONDS PS, WIERZBICKI T, 1978, **Membrane modes for impulsively loaded plates**, Division of Engineering, Brown University Providence, RI 02912.

19. COLE RH, 1948, **Underwater Explosions**, Princeton University Press, Princeton.

20. LIPPMAN, 1974, **Kinetics of the axisymmetric rigid-plastic membrane subject to initial impact**, Int J Mech Sci, Vol 16, pp.297-303.

21. LEE EH, SYMONDS PS, 1952, **Large plastic deformation of beams under transverse impact**, J Appl Mech, Vol 19, pp.308-314.

22. WESTINE PS, BAKER WE, 1974, **Energy solutions for predicting deformation in blast loaded structures**, Proc 16th Explosive Safety Seminar, Hollywood Beach, Florida, USA, pp.849-879.

23. MARTIN JB, SYMONDS PS, 1966, **Mode approximations for impulsively loaded rigid-plastic structures**, J Eng Mech Div, Vol 92, pp.43-66.

24. **Numerical analysis notes**, 1988, AMA 363F.

25. WANG AJ, 1955, **The permanent deflection of a plastic plate under blast loading**, J of Appl Mech, September, pp.375-376.

26. ASHBY MF, JONES DRH, 1985, **Engineering Materials - An introduction to their properties and applications**, Pergamon, pg.30.

27. VOLK, W, 1980, **Applied statistics for engineers**, Robert E Krieger Publishing Company, pp.260-280.

28. HOLMAN JP, 1984, **Experimental methods for engineers**, McGraw-Hill, pp.90-93.

29. PERRONE N, BHAORA P, 1984, **Simplified Large Deflection mode solutions for impulsively loaded, visioplastic, circular membranes**, J of Appl Mech, Vol 51, pp.505-509.

30. SYMONDS PS, JONES N, 1972, **Impulsive loading of fully clamped beams with finite plastic deflections and strain-rate sensitivity**, Int J Mech Sci, Vol 14, pp.49-69.

APPENDIX A TENSILE TESTS

Specimen size was selected from ASTM designation E8-40T where standard sizes are given.

$$\frac{\sigma}{\sigma_o} = 1 + \left[\frac{\dot{\varepsilon}}{\dot{\varepsilon}_o}\right]^{1/n}$$

$$\sigma = \frac{F}{A} \quad \dot{\varepsilon} = \frac{CHS}{L} \times \frac{1}{60}$$

L = gauge length = 2½ inches

Test	Dimensions (mm)	Cross Head Speed (inches/min)	Chart Speed (inches/min)	Yield σ (MPa)	UTS (MPa)	Strain rate $\dot{\varepsilon}$ S^{-1}	Uniaxial Yield σ_o Stress (MPa)
24118801	12,5 x 1,6	0,05	0,5	278,00	352,50	$3,33 \times 10^{-4}$	253,56
25118802	12,5 x 1,6	0,05	0,5	266,88	360,29	$3,33 \times 10^{-4}$	243,41
25118803	12,4 x 1,6	0,2	2	286,97	362,07	$1,33 \times 10^{-3}$	254,60
25118804	12,5 x 1,6	0,2	2	284,67	353,62	$1,33 \times 10^{-3}$	252,55
25118805	12,6 x 1,6	1	10	296,75	367,36	$6,67 \times 10^{-3}$	252,43
25118806	12,3 x 1,6	1	10	305,12	357,11	$6,67 \times 10^{-3}$	259,55
25118807	12,7 x 1,6	5	50	295,51	365,56	$3,33 \times 10^{-2}$	237,90
25118808	12,7 x 1,6	5	50	305,36	374,31	$3,33 \times 10^{-2}$	245,83
25118809	12,5 x 1,6	5	50	378,08	378,08	$1,33 \times 10^{-1}$	314,66
25118810	12,5 x 1,6	20	50	344,19	370,67	$1,33 \times 10^{-1}$	286,46
25118811	12,5 x 1,6	20	50	368,07	368,07	$1,33 \times 10^{-1}$	306,33
SHEET I AVE UTS = 364,51 MPa AVE σ_o = 264,30 MPa							
28098901	12,5 x 1,6	0,05	0,5	302,46	358,06	$3,33 \times 10^{-4}$	275,81
28098902	12,3 x 1,6	0,05	0,5	290,43	363,89	$3,33 \times 10^{-4}$	264,89
28098903	12,3 x 1,6	0,2	2	303,99	365,02	$1,33 \times 10^{-3}$	281,41
28098904	12,3 x 1,6	0,2	2	305,12	365,02	$1,33 \times 10^{-3}$	282,46
28098905	12,3 x 1,6	1	10	342,41	367,28	$6,67 \times 10^{-3}$	291,28
28098906	12,3 x 1,6	1	10	353,72	369,54	$6,67 \times 10^{-3}$	300,90
28098907	12,3 x 1,6	5	50	309,64	372,93	$3,33 \times 10^{-2}$	249,28
28098908	12,3 x 1,6	5	50	316,42	367,28	$3,33 \times 10^{-2}$	254,74
28098909	12,2 x 1,6	20	50	375,19	375,19	$1,33 \times 10^{-1}$	284,36
28098910	12,2 x 1,6	20	50	376,32	376,32	$1,33 \times 10^{-1}$	285,22
SHEET II AVE UTS = 368,05 AVE σ_o = 277,04							

APPENDIX B

Rigid Plastic Analysis (DUFFEY [1])

Assuming a permanent deflection shape (Figure B.1), the maximum deflection of a clamped circular plate subject to a uniform impulsive load is calculated by means of a simplified energy method for a rigid-plastic material behaviour.

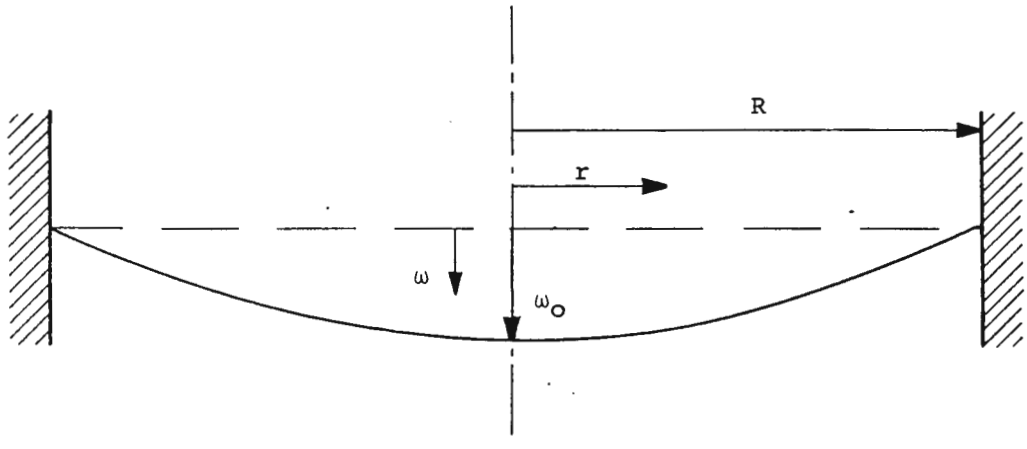

FIGURE B.1 CLAMPED CIRCULAR PLATE AFTER DEFORMATION

The strain energy is calculated as follows:

$$E\rho = \int_v (\int \sigma^{ij}{}_{\varepsilon} d\varepsilon ij) dv \qquad (B.1)$$

From the Kirchoff assumption, $\varepsilon 13$ and $\varepsilon 23$ are zero. In addition, using the plane stress assumption, $\sigma 33 = 0$. Since $\sigma ij = \sigma ji$, the integrand in (3.1) reduces to

$$\sigma^{ij} d\varepsilon ij = \sigma^{11} d\varepsilon_{11} + 2\sigma^{12} d\varepsilon_{12} + \sigma^{22}\, d\varepsilon_{22}$$

Due to symmetry, the shear stress in cylindrical coordinates is zero,

$$\sigma^{12} = \sigma^{r\theta} = 0$$

leaving

$$\sigma^{ij} d\varepsilon ij = \sigma^{11} d\varepsilon_{11} + \sigma^{22} d\varepsilon_{22}$$

Evaluating (B.1), assuming rigid-plastic material behaviour and a proportional stress state,

$$E_\rho = \int_{-t/2}^{t/2} \int_o^{2\pi} \int_o^R [\sigma_{\theta\theta}\, \varepsilon_{\theta\theta} \pm \sigma_{rr}\, \varepsilon_{rr}]\, r dr d\theta dz \qquad (B.2)$$

Strains in the meridional and circumferential directions, respectively, are

$$\varepsilon_{rr} = \varepsilon_{rr_o}(r,\theta) + z\kappa_r(r,\theta) \qquad \text{(B.3)}$$

and

$$\varepsilon_{\theta\theta} = \varepsilon_{\theta\theta_o}(r,\theta) + z\kappa_\theta(r,\theta) \qquad \text{(B.3)}$$

For axisymmetric deformations, the terms in equations (B.3) become functions of r only.

Equations (B.2) and (B.3) therefore give

$$E_p = \int_0^{2\pi} \int_0^{R} \int_{-t/2}^{t/2} \sigma_y \left[\varepsilon_{rr_o}(r) + z\kappa_r(r) + \varepsilon_{\theta\theta_o}(r) + z\kappa_\theta(r) \right] r\,dz\,dr\,d\theta \qquad \text{(B.4)}$$

Integrating (B.4) over θ and z, and assuming $\sigma_{\theta\theta}$ and σ_{rr} are constant,

$$E_p = 2\pi t \int_0^{R} \left[\sigma_{rr}\varepsilon_{rr_o} + \sigma_{\theta\theta}\varepsilon_{\theta\theta_o} \right] r\,dr \qquad \text{(B.5)}$$

Since the cross-section of the plate is assumed to be at constant yield state, and since the stretching strain is the average strain across the thickness of

the plate, the bending contribution to the plastic energy is ignored.

For very large deflections

$$\varepsilon_{rr_o} = \frac{\partial u}{\partial r} + \tfrac{1}{2}\left[\left(\frac{\partial u}{\partial r}\right)^2 + \left(\frac{\partial \omega}{\partial r}\right)^2\right] \tag{B.6}$$

and

$$\varepsilon_{\theta\theta_o} = \frac{u}{r} + \tfrac{1}{2}\left(\frac{u}{r}\right)^2 \tag{B.6}$$

For simplicity it is assumed that there is no displacement in the radial direction, ie. u = 0 which gives:

$$\varepsilon_{rr_o} = \tfrac{1}{2}\left(\frac{\partial \omega}{\partial r}\right)^2 \tag{B.7}$$

and

$$\varepsilon_{\theta\theta_o} = 0 \tag{B.7}$$

Substituting equations (B.7) back into equation (B.5) the plastic strain energy becomes

$$E_p = \pi t \int_0^R \sigma_{rr} \left(\frac{\partial \omega}{\partial r}\right)^2 r\,dr \tag{B.8}$$

Utilising the Hencky deformation theory of plasticity that there is a one to one correspondence between stress and strain, the location of the yield surface in stress space can be determined as the intersection of the elastic radial line from the origin of stress space and yield surface.

In the elastic region,

$$\varepsilon_{\theta\theta_o} = \frac{1}{E}(\sigma_{\theta\theta} - \nu\sigma_{rr}) \qquad \text{(B.9)}$$

From equation (B.7)

$$\varepsilon_{\theta\theta_o} = 0$$

which gives from equation (B.9) that

$$\sigma_{\theta\theta} = \nu\sigma_{rr} \qquad \text{(B.10)}$$

Invoking the Von Mises yield condition that

$$\sigma_{rr}^2 - \sigma_{rr}\sigma_{\theta\theta} + \sigma_{\theta\theta}^2 = \sigma_y^2 \qquad \text{(B.11)}$$

Where σ_y is the yield stress in simple tension, and substituting (B101), the radial yield stress is

$$\sigma_{rr} = \frac{\sigma_y}{(1-\nu+\nu^2)^{\frac{1}{2}}} \qquad \text{(B.12)}$$

APPENDIX C
DYNAMIC YIELD STRESS VALUES

$$\frac{I^2\ 96421,8}{\sqrt{\sigma_o{}^1}} = 40\ (\frac{\sigma_o{}^1}{\sigma_o} - 1)^5$$

Test No	Static Yield Stress σ_o (MPa)	Impulse (N.s)	Dynamic Yield Stress $\sigma_o{}^1$ (MPa)
210903	264,30	4,76	571,84
041006	277,04	13,28	749,37
041005	277,04	16,85	793,61
041004	277,04	17,75	803,73
041003	277,04	18,65	813,63
041002	277,04	17,75	803,73
041001	277,04	21,69	844,82
041007	277,04	24,56	871,95
041008	277,04	24,24	912,01
051002	277,04	26,34	887,79
051005	277,04	26,17	886,27
051008	277,04	25,63	881,52
051009	277,04	28,15	903,05
051010	277,04	28,86	909,05
051003	277,04	29,77	916,29
051004	277,04	30,67	923,48
041009	277,04	29,41	913,45
051001	277,04	30,31	920,69
061002	277,04	32,48	932,54
220901	264,30	32,66	898,49
101101	277,04	34,29	950,96
250901	264,30	36,65	927,37
220902	264,30	40,48	951,37
270902	264,30	36,65	927,37
270901	264,30	37,37	931,17
250902	264,30	37,57	932,48
061001	277,04	39,56	987,95
101102	277,04	37,75	975,58
250903	264,30	41,37	957,02
250904	264.30	39,38	944,37
250905	264,30	42,12	961,60
250906	264,30	42,46	964,98
101103	277,04	43,58	1 014,08
061004	277,04	49,64	1 050,71
250907	264,30	49,46	1 004,65
270903	264,30	47,25	992,91
101104	277,04	46,88	1 034,43
061005	277,04	48,53	1 044,27
101105	277,04	52,05	1 064,49

APPENDIX D

PREDICTION OF A POLYNOMIAL USING STIRLING'S FORMULA

Using node shape functions predicted by Nurick [13]

	x		y		Δ		Δ^2		Δ^3		Δ^4		Δ^5
	0		1		-0,066								
	10		0,934	$f_{-\frac{1}{2}}$	-0,164		-0,098	$f^3_{-\frac{1}{2}}$	0,027				
x_o	20	f_o	0,770	$f_{\frac{1}{2}}$	-0,235	f_o^2	-0,071	$f^3_{\frac{1}{2}}$	0,035	f_o^4	0,008		0
	30		0,535		-0,271		-0,036		0,043		0,008		
	40		0,264		-0,264		0,007						
	50		0										

$f(x)$ of order 4 $\qquad \theta = (\frac{x - x_o}{h})$

Let $\qquad x_o = 20 \qquad \theta = \frac{x - 20}{10}$

$$f(x)=f_o+\theta\mu\delta f_o + \frac{1}{2!}\theta^2\delta^2 f_o^2 + \frac{1}{3!}\theta(\theta^2-1)\mu\delta^3 f_o + \frac{1}{4!}\theta^2(\theta^2-1)\delta^4 f_o$$

$$\mu\delta^n f_o = \tfrac{1}{2}(\delta^n f_{-\frac{1}{2}} + \delta^n f_{\frac{1}{2}})$$

Therefore

$$f(x) = 0,770 - 0,20467\ (\frac{x-20}{10}) - 0,03583\ (\frac{x-20}{10})^2 + 0,00517\ (\frac{x-20}{10})^3 + 0,00033\ (\frac{x-20}{10})^4$$

Therefore the shape function is

$$\omega = \omega_o \quad (f(x))$$

APPENDIX E

CONFIDENCE LIMITS OF SLOPE AND LEAST-SQUARES LINE [27]

Input Energy: correlation coefficient r = 0,9989

Equation of straight line $\log E_{input} = 0,3230 + 1,955 \log\phi$

[$\log E_{input}$ vs $\log \phi$]

90% confidence range of $\log \overline{E}_{input} = 3,816 \pm 0,003$

90% confidence range of slope = $1,955 \pm 0,029$

Deformation Energy: correlation coefficient r = 0,9310

Equation of straight line $E_{def} = -3349,74 + \frac{324813,5}{\phi}$

[E_{def} vs $\frac{1}{\phi}$]

90% confidence range of $\overline{E}_{def} = 1462,12 \pm 70,23$

90% confidence range of slope = $324813,5 \pm 28477,3$

Tearing Energy: correlation coefficient r = 0,889

Equation of straight line $E_{tear} = 124,22\phi - 5896,9$

90% confidence range of $\overline{E}_{tear} = 2707,09 \pm 298,98$

90% confidence range of slope = $124,22 \pm 27,07$

Disc Energy: correlation coefficient r = 0,912

Equation of straight line E_{disc} = 175,96 O - 7692,0

90% confidence range of E_{disc} = 4278,3 $\pm$ 352,0

90% confidence range of slope = 175,96 $\pm$ 31,47

APPENDIX F : CALCULATION OF MAXIMUM STRAIN RATE

Using the Cowper-Symonds equation:

$$\frac{\sigma_o{}^1}{\sigma_o} = 1 + \left(\frac{\dot{\varepsilon}}{\dot{\varepsilon}_o}\right)^{1/n}$$

with

$n = 5$

$\dot{\varepsilon}_o = 40 \text{ sec}^{-1}$

$\sigma_o = 277{,}04 \text{ MPa}$

The Dynamic yield stress is determined by using the relation given in equation 3.11 and is

$$\sigma_o{}^1 = 1064{,}49 \text{ MPa}$$

$$\frac{1064{,}49}{277{,}04} = 1 + \left(\frac{\dot{\varepsilon}}{40}\right)^{1/5}$$

Therefore

$$\dot{\varepsilon} = 7421 \text{ sec}^{-1}$$

APPENDIX G

COURSES COMPLETED FOR PARTIAL FULFILMENT OF THE REQUIREMENTS FOR THE DEGREE OF MASTER OF SCIENCE

CIV 588F	- APPLIED MECHANICS I	3 credits
CIV 589F	- APPLIED MECHANICS II	3 credits
CIV 540F	- FINITE ELEMENT ANALYSIS	4 credits
AMA 363F	- NUMERICAL ANALYSIS	3 credits
AMA 367F	- CONTINUUM MECHANICS	3 credits
CIV 525S	- CONTRACT LAW	2 credits
MEC 5202	- PROJECT MANAGEMENT	2 credits
	TOTAL :	20 credits